University Of California, Merced

INVESTIGATION AND APPLICATION OF CRYSTAL PHASE BEHAVIOR TO OBTAIN ENANTIOPURE CHEMICALS

A Thesis submitted in partial satisfaction of the requirements

for the degree of Master of Science

in

Chemistry and Chemical Biology

by

Ivy Kathleen Price

Committee in charge:

Professor Jason Hein
Professor Matthew Meyer
Professor Uttam Tambar

2014

The Thesis of Ivy Kathleen Price is approved, and it is acceptable in quality and form for publication on microfilm and electronically:

_____

Jason Hein

_____

Matthew Meyer

_____

Uttam Tambar

_____

Erin Johnson, Chair

University of California, Merced

2014

Dedication

I would like to dedicate this thesis work to my parents, Rusty and Mary Margaret. Thank you for always supporting my decisions and goals, no matter how crazy they may seem. Your love and support mean the world to me and I could not have made it this far, both literally and figuratively, without y'all. I would also like to dedicate this work to the memory of my granny, Linda, who sparked my passion for education.

Table of Contents

List of Figures

List of Equations

Acknowledgements

I would like to thank the Chemistry and Chemical Biology group at the University of California, Merced for the opportunity to further my education. Thank you for providing amazing opportunities for growth as a researcher and as an educator.

I would like to extend my deepest gratitude to my committee members, Dr. Erin Johnson, Dr. Matthew Meyer, and Dr. Uttam Tambar. Thank you for your insights, time, and effort in guiding my education and research.

To my advisor and committee member, Dr. Jason Hein- thanks for your patience and your willingness to have me as a student in your lab. Your passion for research and chemistry education is contagious.

I'd also like to thank my fellow Hein lab graduate group members, Diana Yu and Matt Berry, for their support, encouragement, and lots of laughter. You guys have been a joy to work with and I believe the friendships formed will last a lifetime.

I would also like to thank the current post-doc in the Hein lab, Dr. Celine Rouget. Thank you for all the training and for teaching me so much about crystallizations.

Thanks goes out to past and current Hein lab group members: Blessing Cao, Disnay Castrejon, Sumindar Kuhr, Indyana Polley, Van Thai, Ruben Vargas, and Ahn Vo. Thanks for the awesome lab environment.

I'd like to thank those friends who have helped California become a home away from home and have provided such a great support system during my time at UC Merced. This includes (but is not limited to): Drew Abney, Josh Baker, Chelsea Carey, Kevin Clancy, Shanna Erickson, Rebecca Lever, Emma McCorkle, Merced Running Club members, Elizabeth Owens, and Luke Reed.

To my family, thank you for supporting me in this endeavor, for not pressuring me either way in any of my decisions and for helping me move out to California. Without y'alls unconditional love, I would not be who I am today.

Finally, I would like to thank the University of California, Merced and the National Science Foundation (NSF) grant number CHE-1300686 for research and educational funding. Without them, research and education would not have been possible.

Abstract of the Thesis

INVESTIGATION AND APPLICATION OF CRYSTAL PHASE BEHAVIOR TO OBTAIN ENANTIOPURE CHEMICALS

by

Ivy Kathleen Price

Master of Science, Chemistry and Chemical Biology

University of California, Merced, 2014

Dr. Erin Johnson, Chair

An efficient method of creating and separating chiral molecules into enantiomers is a problem facing synthetic chemistry. Currently, most research is focused on creating enantiopure materials via asymmetric synthesis. The goal of this thesis project is to develop preferential crystallization techniques, specifically for crystalline materials, which form heterochiral (racemate) systems. Before this can be attempted, detailed information of the relative stability of possible crystal forms, including homochiral and heterochiral solid phase (known as conglomerate and racemate crystals), needs to be obtained.

This thesis focuses on several crystallization techniques that can be used to separate enantiomers using both one pot and two pot methods as well as a new method known as thermal ripening. Some systems merely use a seed crystal as the driving force for separation, while others use a slight offset of equilibria in an epimerizing system. Solubility differences in heterochiral and homochiral crystal forms also play a role in separations. By further understanding and establishing control over systems like these, we are gaining ground towards developing efficient methodology to separate chiral systems which will benefit both the industrial and research worlds.

Chapter 1:

New modes of Enantiopurification Using Dynamic Preferential Crystallization: Application to the Synthesis of Naproxen

Abstract:

Naproxen methyl ester has been subjected to two new enantiopurification techniques. Both of these take advantage of crystallization of the enantiomers as separate crystals (conglomerates) and utilize solution phase racemization to interconvert the two enantiomers. These two techniques are meant to address limitations in current dynamic resolution techniques, specifically for systems that require extended processing time to reach enatiopurity. The first utilizes a protype apparatus that contains two different crystallization zones and mass transfer via a homogenous liquid phase. The second uses a single flask and a programmable temperature ramps to effect alternating dissolution and re-accretion. In the end, both techniques prove to be viable alternatives to attrition enhanced deracemization using abrasive grinding and are more amenable to scale up for industrial application

Introduction

1.1 Chirality, Enantiomers and You

Any molecule that is non-superimposable on its mirror image is said to be chiral. A chiral center is one in which four different attachments come off from a central carbon. This is also known as an asymmetric center. A pair of molecules that are non-superimposable mirror images are known as enantiomers (IUPAC, 1997) Because of the mirror symmetry, enantiomers possess identical physical properties such as boiling point, melting point, reactivity with achiral molecules, and solubility. However, pairs of enantiomers do possess differing chemical properties, i.e. reactivity with chiral molecules because of their spatial arrangement. The amino acids and carbohydrates that are the building blocks for the proteins, polysaccharides and nucleic acids in all biosystems are present only as single enantiomers. Because of this, pure chiral molecules are of utmost importance in the pharmaceutical industry, as chiral molecular interaction can be vastly different depending on the particular enantiomer involved. For example, smell receptors, which are composed on amino acids, are chiral entities, allowing us to discriminate enantiomers. One striking case of this phenomenon is seen with (R)-carvone, which smells like spearmint, while the (S) enantiomer smells like caraway (Leitereg, 1971).

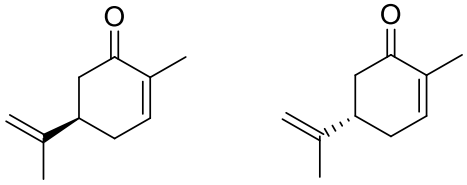

(R) – carvone spearmint

(S) – carvone caraway

Figure 1-1: Structures of carvone enantiomers.

1.2 The Discovery of Stereoisomers

At the beginning of the eighteenth century, a French mineralogist, René-Just Haüy, discovered that quartz crystals could exhibit mirror image dimensions (Kunz, 1918). Around the same time, in 1831 Jean Baptiste Biot, discovered that a beam of polarized light passing through a chiral substrate could be rotated either clockwise or counter-clockwise (Lakhtakia, 1990). One such compound Biot was studying was tartaric acid, which is found naturally in such plants as grapes, bananas, and tamarinds. Naturally extracted

tartaric acid could indeed rotate polarized light but the ammonium salt of tartaric acid, which was of interest to Louis Pasteur, could not.

In 1848 Pasteur crystallized an ammonium salt of tartaric acid and was curious at why naturally extracted tartaric acid would rotate light, but what seemed like the identical molecule synthesis in the lab would not (Pasteur, 1848). More, interestingly, Pasteur discovered that crystals obtained from the lab-synthesized tartaric acid were made up of two discernable populations of crystals, which were nearly identical except for being mirror images of each other. Using a microscope, he then proceeded to carefully separate the two different crystal forms by hand using a pair of tweezers. Once he had the crystal forms separated, he noticed that individual solutions created from each pile of the separated crystals would indeed rotate light, but in opposite directions. Thus, the first mechanical separation of single enantiomers is credited to Pasteur. In addition, a long standing mystery regarding the origin of optical rotation had been solved. From a practical standpoint though, the mechanical separation of racemic mixtures with tweezers is ridiculous. Many methods have been developed since Pasteur's initial work in hopes of addressing this challenging problem as well as methods in current development.

1.3 Crystal Habits of Enantiomers

Two types of crystal forms that will be discussed are racemate and conglomerate forms. A conglomerate compound has only one enantiomer within its unit cell. By contrast, a racemic crystal will form with both enantiomers within its unit cell.

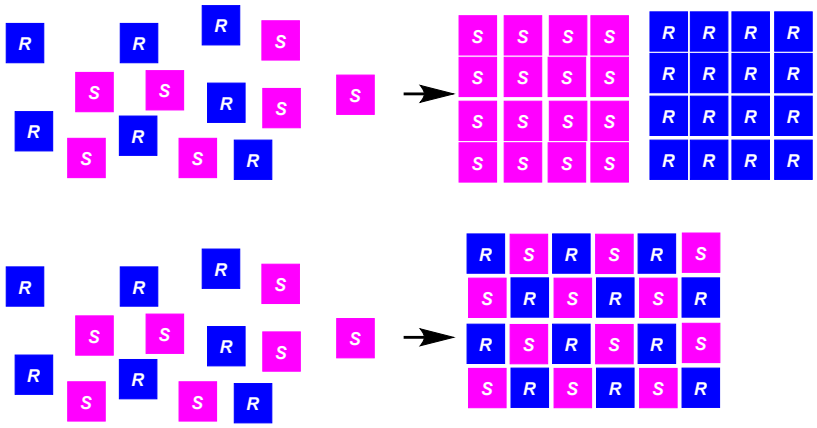

Figure 1-2: Schematic of conglomerate (top) and racemic (bottom) crystal forms.

Technically, one could have a mechanical racemic mixture of a conglomerate compound, having both enantiomers present in the mixture but only a single enantiomer in each crystal. This was the case with the aforementioned crystallization carried out by Pasteur and why a mechanical separation was even possible.

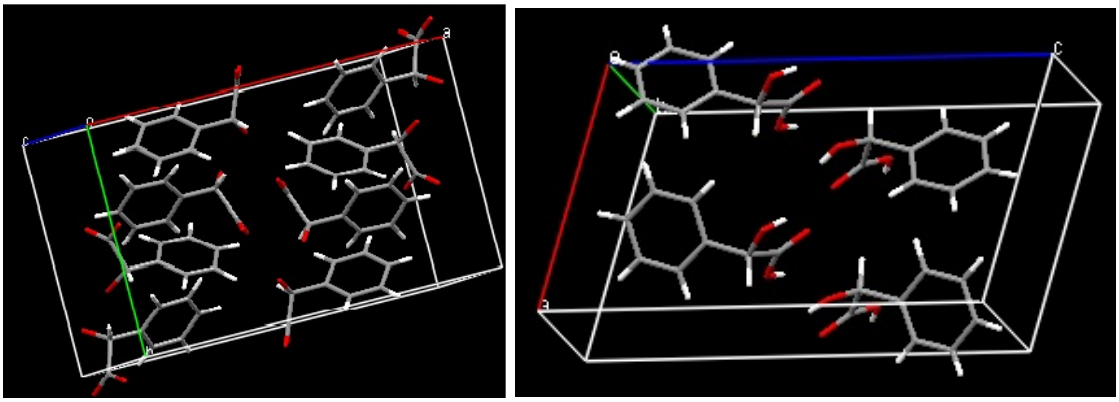

Figure 1-3: Unit cell of a racemic crystal (left) versus a conglomerate crystal (right) for mandelic acid.

The measurement of purity of chiral substances is known as enantiomeric excess (*ee*). It shows a percentage of which enantiomer the chiral substance is biased towards. For example, the enantiomeric excess of a racemic substance is 0%, while an *ee* of 100% refers to an enantiopure compound. EE is calculated by the following equation.

$$ee = \frac{|[R]-[S]|}{[R]+[S]} \times 100 \qquad (1)$$

1.4 Obtaining Enantiopure Materials Using Crystallization

The main practice of obtaining enantiopure material currently is through asymmetric synthesis. This is where a chemical reaction or series of reactions produces a specific enantiomer or diasteriomer. There are several techniques in obtaining enantiopure material from a non-synthetic perspective. These include attrition enhanced deracemization, coupled preferential crystallization, Auto Seeded Polythermic Programmable Preferential Crystallization (AS3PC), preferential crystallization via a metastable conglomerate, and Second Order Asymmetric Transformation

(SOAT) (Levilain, 2010) No method is perfect, as each has its own advantages and disadvantages. A few methods will be discussed further.

1.4.1 Preferential Crystallization

Solubility is defined as the amount of a compound that can be dissolved in a liquid phase at a given temperature at its equilibrium point. If the amount of material dissolved is greater than the solubility equilibrium permits then the solution is said to be supersaturated or metastable. Preferential crystallization techniques depend upon these metastable limits and solubility properties (Jacques, 1994).

In order for crystals to grow in the first place, a supersaturated system is required. This provides the driving force necessary to formed molecules from the solution phase to the growing solids. This is all that is required to affect crystal growth, but the system must already have a solid phase composed on some crystalline material present. If the solution is homogenous the solution phase supersaturation may not necessarily lead to the formation of new crystals. In this case a new crystal phase usually must meet the metastability limit in order for nucleation to occur. Nucleation is the initial step in the formation of a new crystal, onto which a crystal phase can grow. As long as a solution's temperature-concentration profile is within the metastable zone, which is defined as the region between the solubility limit and the highest recorded concentration and temperature where crystals reliably appear, nucleation can occur. Factors affecting nucleation are complex and highly system dependent. While this will not be the focus of this discussion many studies examining controlling this phenomenon can be found. (Levilain, 2010)

A diagrammatic representation of the crystallization process is illustrated in figure 1-4. A solution is initially at a temperature and concentration such that all material is in solution (Point A). This is represented because the value on the graph is below the solubility limit. If this sample were to be cooled the concentration would remain invariant (A to B). The solution would cross over the solubility line and enter the metastable region. At this point the solution is said to be supersaturated. Cooling could continue until the system reaches the metastability limit (Point B), at which time nucleation occurs and crystals form. Crystallization then occurs until the sample returns to the solubility limit (B to C) and the system is again at equilibrium (Point C). Generally, enantiopure conglomerate crystals have a lower solubility than racemic conglomerate crystals, meaning nucleation of enantiopure crystals would occur first, allowing preferential crystallization of just a single enantiomer.

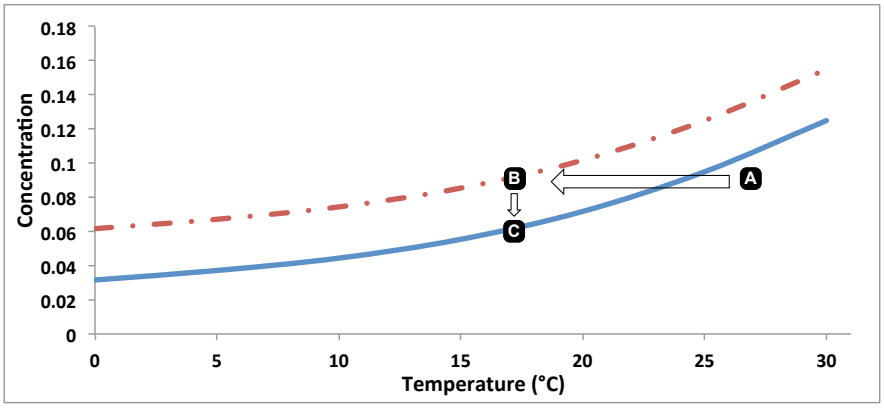

Figure 1-4: Diagram of crystallization process. This diagram shows the hypothetical solubility limit (blue line) and metastability limit (red line) for a compound. Points A, B, and C represent events during a cooling crystallization from a homogenous starting point.

Due to these two important boundary conditions (the metastability limit and the solubility limit) it is possible to selectively crystalize one enantiomer away from another if two important conditions are met. First the solution must be homogenous and then brought into the metastability region. This creates a conditions so that crystals *could* grow, however no nucleation has yet occurred. Second, a nucleation seed of only one enantiomer is added so that a single enantiomer will accrete from the solution phase onto this seed. This preferentially depletes the seeded enantiomer from the solution phase and allows it to be isolated as a single pure crystal.

1.4.2 Attrition Enhanced Deracemization

Recently, a new method of dynamic resolution known as attrition enhanced deracemization has been developed. This technique utilizes a saturated slurry containing a nearly racemic mixtures of conglomerate crystals. Once the solubility equilibrium has been establish, a racemization catalyst is introduced allowing the two enantiomers to interconvert in the solution phase (Figure 1-5). If a slight excess of one conglomerate exists, the probability of crystallization will be different for each enantiomer. This results in net mass transfer (Figure 1-5; from S to R), leading to growth of the major enantiomer at the expense of the minor. The overall process allows an initially racemic mixture to be converted completely to a homochiral solid phase. While powerful, this technique is limited to compounds which preferentially form conglomerate crystals and contain a stereocenter that is readily epimerized in the solution phase. Since an estimated 90% of chiral compounds form stable heterochiral solid phases, known as racemate crystals, general application of this method has been restricted (Lorenz et al., 2006).

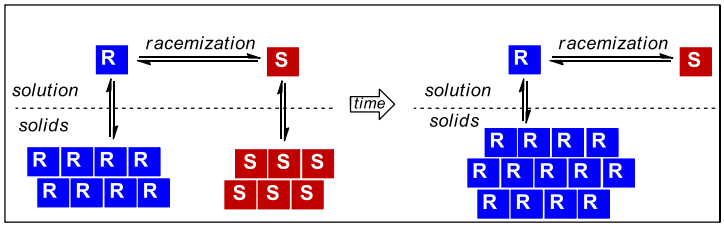

Figure 1-5: Schematic of the progress of deracemization with time.

Cristobal Viedma was the first to do work on attrition enhanced deracemization. In his work, he describes breaking chiral symmetry of D and L sodium chlorate crystals via attrition (Viedma, 2004)

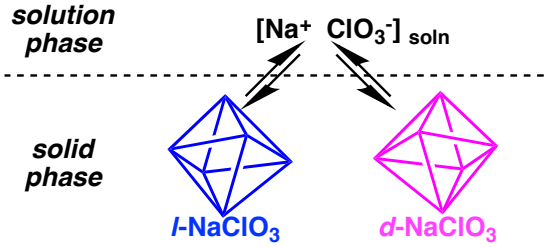

Figure 1-6: Sodium chlorate retains chirality in the solid phase and loses chirality when it dissolves.

The foundation for this symmetry breaking is due to the chemical equilibrium shown above. Once dissolved in the solution phase the sodium chlorate crystals lose chirality. Therefore, there is an equal probability of either enantiomer crystallizing back out of solution. This work proves that basically more attrition means faster breaking of symmetry when there is an initial imbalance or slight enantiomeric excess. Higher stir rates also affect the rate at which the racemic system becomes enantiopure. It was also found that grinding the system (stirring with glass beads) had the same effect but evolution of slid phase e.e. increased at an even faster rate than what was originally discovered with just a stir bar at a fast rate. Enantiopure samples of sodium chlorate could be accessed in about 10 hours using 8 grams of glass beads to agitate the system. This is possible because when dissolved in solution sodium chlorate 'forgets' what chirality it is, otherwise coined as chiral amnesia (Blackmond, 2007). Chiral amnesia is thought to be the driving force for solid-phase homochirality. Then it crystallizes out as whichever enantiomer the solid phase is biased more in or which way the equilibria of the solid phase lies. The solid phase equilibria is offset and thus drives the crystallization of the enantiomer in which the solid phase is biased.

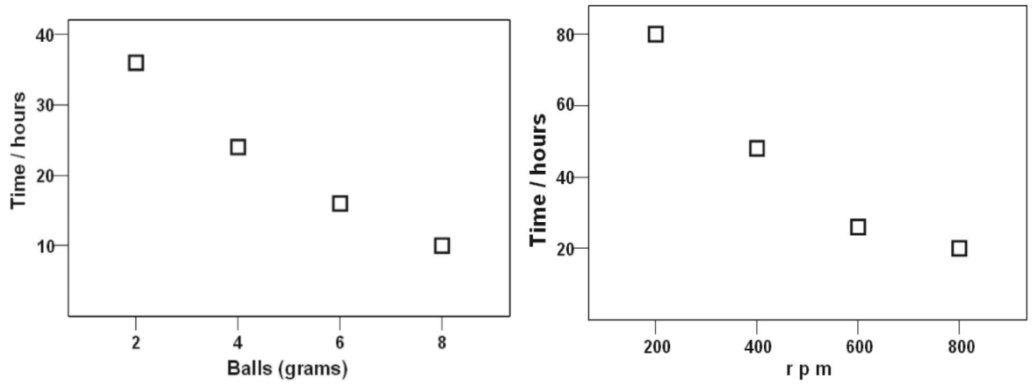

Figure 1-7: The effects of attrition with differing amounts of glass balls and differing stir rates (reprinted from Viedma, 2005). These graphs show the total time required for racemic suspensions to reach enantiopurity when subjected to grinding.

Applying attrition enhanced deracemization requires abrasive grinding during the process. This presents several problems from an application standpoint. First the mechanical force necessary to stir a tank filled with an abrasive agents increases dramatically as the size of the reactor goes up. Second, there is always a chance that small amounts of the abrasive material will remain in the final crystalline product.

The question then turns to why grinding is necessary at all. Resolution enhanced by attrition is fundamentally driven by Ostwald Ripening. Ostwald Ripening states that the smaller the crystals are, the more likely each will be to dissolve, rather than grow, giving each crystal greater probability to go into solution (Liesegang, 1911). If small crystals were to dissolve a momentary supersaturation would exist leading to a new driving force to re-accrete material on another crystal in the system. Thus, a system will tend to form larger crystals at the expense of smaller ones (Ostwald, 1896). This theory is in accordance with the Gibbs Thompson Effect, and explains crystal size dependence in relation to solubility. The Gibb Thompson equation can be written below, where C(L) is the concentration of a crystal of size L, $C\infty$ is the solubility of the material made up of an infinitely long plane (Gibbs, 1948).

$$C(L) = C_\infty \exp(\alpha/L) \qquad (2)$$

Thus grinding may help to promote deracemization by keeping the nascent particles in the system very small and highly solubly. This pushes the system to a state which is temporarily supersaturated relative to the crystal size of the particles present.

A second benefit to grinding a crystal sample is simply the promotion of mass transport between crystal populations. This has been demonstrated using an isotopic labeling study, where a ^{15}N isotopically enriched compound was added to a saturated solution containing the molecule with a ^{14}N isotope (Hein et al., 2012) Stirring the solution mildly led to a very slow rate of exchange between the molecule in the solid and solution phase, while grinding the sample rapidly allowed the isotope to be evenly distributed between both solid and liquid in only a few hours.

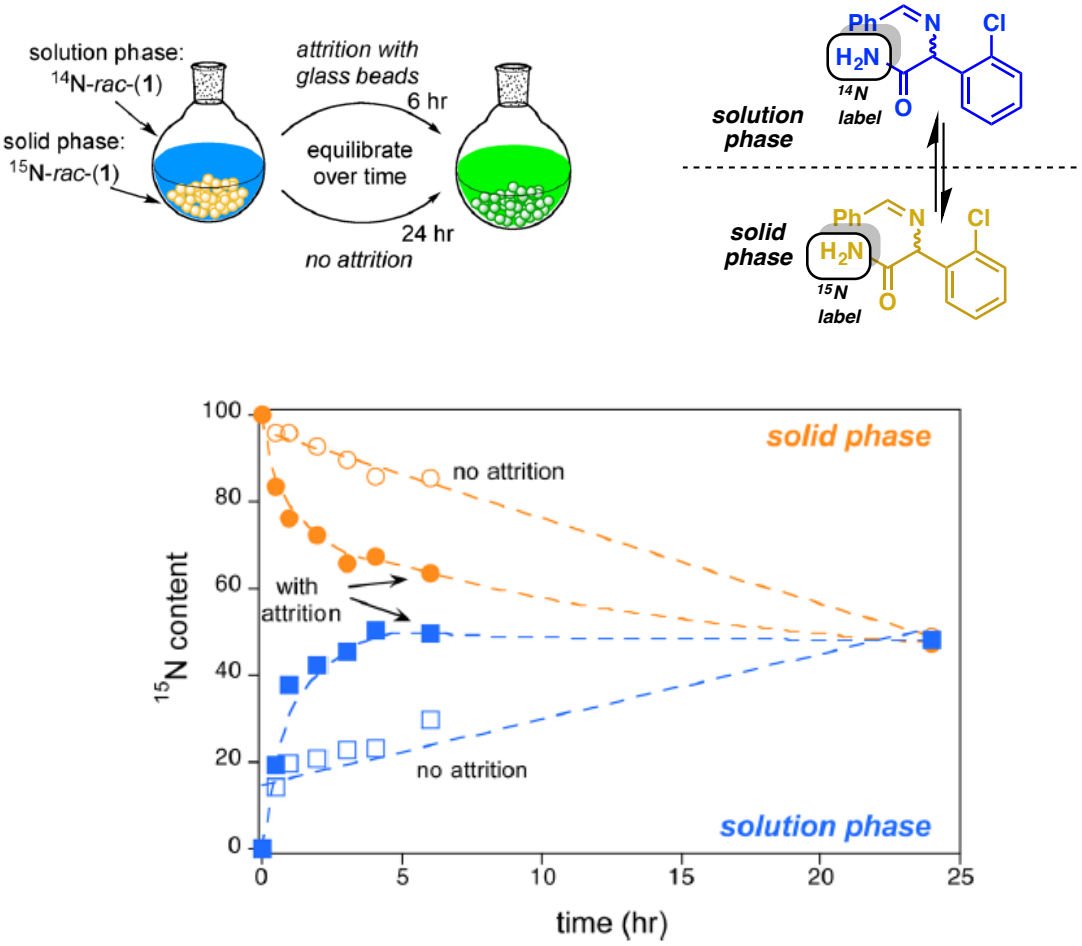

Figure 1-8: Effects of attrition on the rate of mass transfer (From Hein, JACS 2012). Experiment used 14N or 15N labeled imine shown above

1.4.3 Coupled Preferential Crystallization

Coupled preferential crystallization is a method that can provide both the necessary mass transport as well as the differing solubility environments needed to allow dissolution, racemization and re-accretion as a new crystal

form. Initial experiments in our lab were aimed at developing new methods to separate non-racemizable conglomerate crystals. This was accomplished using a prototype apparatus incorporating two flasks connected by a fluid pumping system (Fig. 1-9). Initially, a saturated slurry is created in Flask A with Flask B being seeded with a single enantiomer. The temperature of A is set slightly greater than B and the solution phase is circulated, using filters to prevent solid phase movement. As solvent is withdrawn from A (Fig. 1-9, Point 1) the concentrations of both enantiomers are equal, giving rise to a racemic solution. Once in Flask B, the lower temperature results in a slightly supersaturated solution in contact with only one crystal form. This provides a sufficient driving force to permit growth of the seeded enantiomer without allowing nucleation of other. The solution being returned to A (Fig. 1-9, Point 2) now shows a slight depletion of the seeded compound and over time results in complete separation of the two enantiomers. While conceptually simple, successful resolution requires tight control over the solubility equilibria and an understanding of the metastability of the solid phases, thus identifying operational parameters can be very challenging. By applying real-time in situ monitoring we were able to rapidly identify optimal conditions (flow rate, temperature difference, rate of crystallization etc.) and develop protocols to separate conglomerate pharmaceuticals such as Omeprazole, Naproxen and Plavex (Noorduin, 2010; Hein, 2012; Kaptein, 2009) .

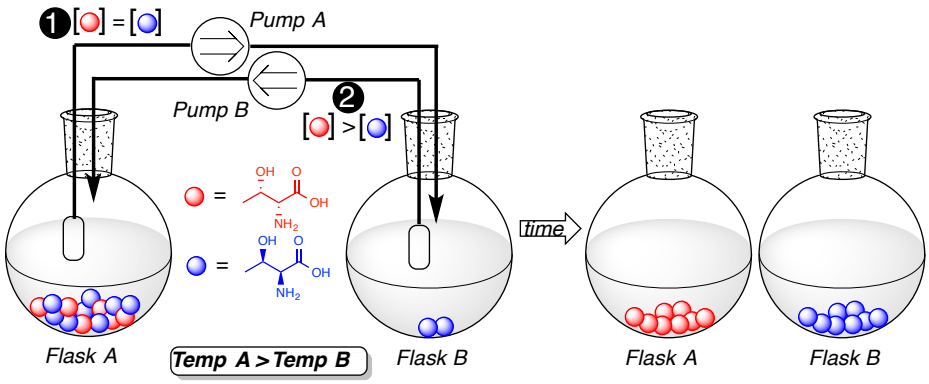

Figure 1-9: Schematic of coupled preferential crystallization set up. Two flask pump system used in coupled preferential crystallizations. Flask B is seeded with single enantiomer conglomerate crystals and set at a slightly cooler temperature to promote crystal growth.

Preferential crystallization methods, as stated earlier, do not involve a chemical change of the molecule but conditions are implemented so that one enantiomer crystallizes away from the mixture leaving enantiopure crystals in one flask. For this to occur, a two or three flask system connected via a

pump must be used and seed crystals of one enantiomer need to be added to offset the equilibrium and drive the crystallization process.

1.4.4 Combined Coupled Preferential Crystallization with In Situ Racemization

Attrition enhanced deracemization is efficient on small scale but is quite problematic when scaled for industrial processing. There needs to be a vessel that can withstand the force of the grinding beads and thus, leads to a greater chance of a vessel bursting. More solvent is also needed to wash the beads in order to get most of the material back. This method is rather wasteful on a large scale and is not practical. There are a few logistical problems that occur when scaling up to industrial scale. For one, sonication generates a lot of heat which could cause decomposition to occur in some molecules. With attrition via glass beads or another form of grinding mechanism there is the issue of the vessel being able to withstand the violent abrasive agitation on the kilogram scale. In addition, stirring large beds of beads requires unrealistically large mechanical torque if large plant reactors were used. Finally, there is the issue of contamination of the final crystal product with other insoluble materials from break down of the grinding element, such as pieces of silica glass or metal fragments.

One other problem with attrition enhanced deracemization is indiscriminate attrition. During the process both the desired and undesired enantiomer are subjected to grinding, leading to destruction of both the material you are trying to remove and the sample you are trying to grow. One solution is to separate these two processes into two flasks. Recently the Kaptein (2009) group reported findings in a study of the deracemization of naproxen and were able to produce enantiopure naproxen within six days by only adding base to promote epimerization and by applying abrasive grinding to the system.The lack of efficiency in this example is a perfect test case for the two-zone technique.

Results and Discussion

1.5 Studies on Naproxen Methyl Ester and Hypotheses

Our group desired to implement softer, more conservative conditions with no abrasive grinding so as to market how the system could be scaled up to the industrial level. This was accomplished using two different approaches. First, we implemented a racemization method using a two pot pump system with the EasyMax workstation, a conservative stir rate, and a small

temperature differential for the deracemization of racemic naproxen to enantiopure naproxen. A second method to be discussed is breaking enantiomeric symmetry by a using a series of temperature oscillations in a one pot system.

For this study naproxen methyl ester was selected as a model system to study for two reasons. First, we know that while Naproxen crystallizes as a racemate, the methyl ester of naproxen is easily accessed and crystallizes as a conglomerate (Kaptein et al., 2009). Second, this compound has successfully been applied to attrition enhanced deracemization, however, the process took many days. We mainly attribute this lack of progress to the relatively slow rate of epimerization of the two enantiomers in the solution phase. (Kaptein et al., 2009) We predict that using a two pot attrition enhanced deracemization will obtain enantiopure crystals more efficiently than previously done.

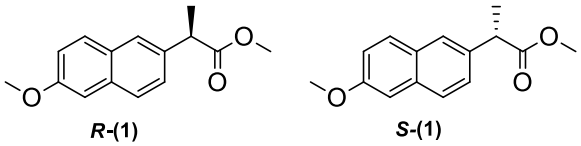

Figure 1-10: Enantiomers of 2-(6-Methoxy-2-naphthyl) propanoic acid.

1.6 Solubility Profile of Naproxen Methyl Ester

Before any crystallization studies can occur, one must first have an understanding of the solubility behavior. Knowing the amount of material that can dissolve at any given temperature allows up to pick an appropriate working temperature range, such that we have enough material in solution to carry out the epimerization chemistry, but also not dissolve too much of our crystal phase. In addition, we need to know that we are creating a supersaturated solution, even transiently, in order for any crystallization to occur. Without this information, we may not be able to set up the experiment such that we maintain a saturated system, and thus all crystals would be lost leading to a homogenous system, and no crystal phase to utilize.

For this, we first measured the solubility profile of both the racemic and the enantiopure naproxen methyl ester by IR. From this profile, we can better plan experiments in order to prevent spontaneous nucleation of the undesired enantiomer by setting the temperature differential in each vessel so that this does not occur. The single enantiomer has a much lower solubility than that of the racemate so it will crystallize out of solution before the racemate. This phenomena helps the separation.

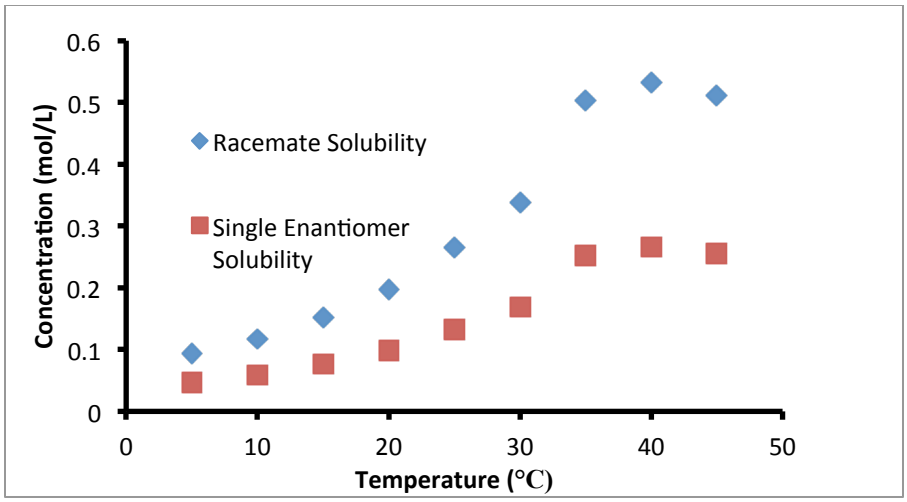

Figure 1-11: Solubility Curve of Naproxen Methyl Ester. Information on the solubility behavior of racemic-*1* was obtained from the Mettler Toledo Easy Max Synthesis Workstation and the Mettler Toledo ic10 ReactIR. See Appendix III for experimental details.

1.7 Rate of Epimerization

This slow epimerization of naproxen methyl ester complicates purification (Kaptein et al., 2009). Ideally, one would want rapid epimerization to occur in the solution phase so that when seeded with one enantiomer, any crystal growth (or depletion of a single enantiomer from the solution phase) would immediately be reset by way of a fast chemical epimerization. This would mean the solution phase is always racemic and there would not be a build up of any one enantiomer. If this condition is maintained the system should give a higher probability of crystallizing out onto its appropriate enantiomer.

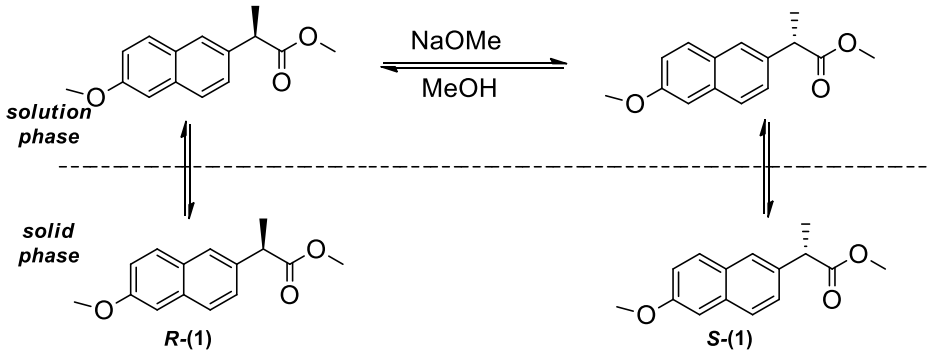

Figure 1-12: Scheme of epimerization reaction of naproxen methyl ester and crystallization.

Also, with a rapidly epimerizing system rate of crystallization seems not to be such an important aspect to consider. If the rate of crystallization of one enantiomer vastly outpaced the rate of epimerization a large excess of one enantiomer would be left in solution leading to possible nucleation of the wrong enantiomer.

In order to confirm that the rate of epimerization was indeed slow we measured the rate at which an enantiopure sample became racemic with differing amounts of base and at different temperatures. For these experiments we began with a homogenous solution of a single enantiomer. At time = 0 base was added as a solid and then samples were withdrawn at time points and quenched into MeOH with 0.1 M HCl to stop epimerization. These time points were analyzes offline by chiral HPLC, and the enantiomeric excess was recorded

In this system, epimerization is occurring by deprotonation at the chiral benzylic center of naproxen to form an achiral enolate. Proton capture is non-specific allowing either the R, or S enantiomer of naproxen to form. Thus we expect the rate of the erosion in e.e. to decrease as the sample approaches a racemic mixture. This process is simply an approach to equilibrium and will display a first-order profile.

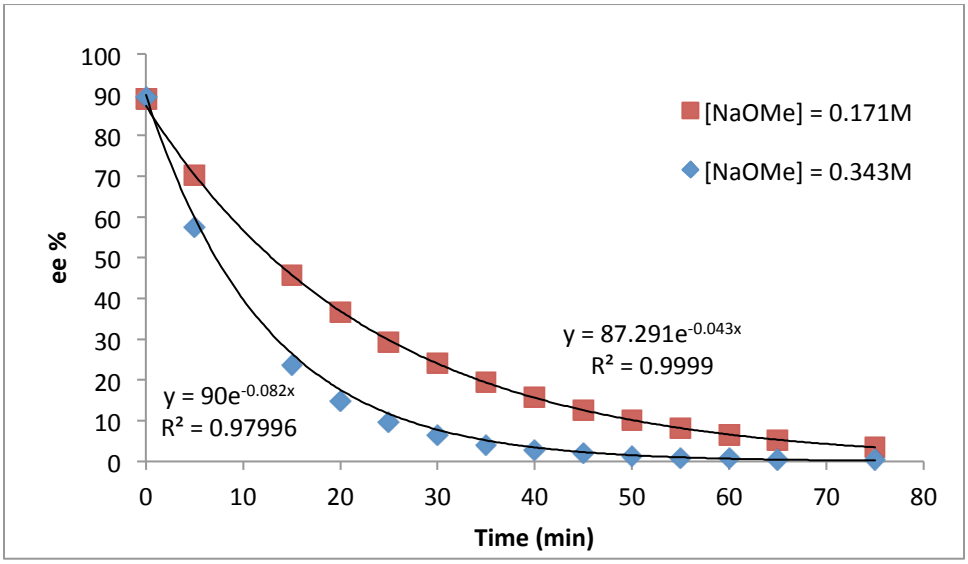

Figure 1-13: Rate of epimerization experiment at 45°C with varying concentrations of NaOMe.. See Appendix V for experimental details.

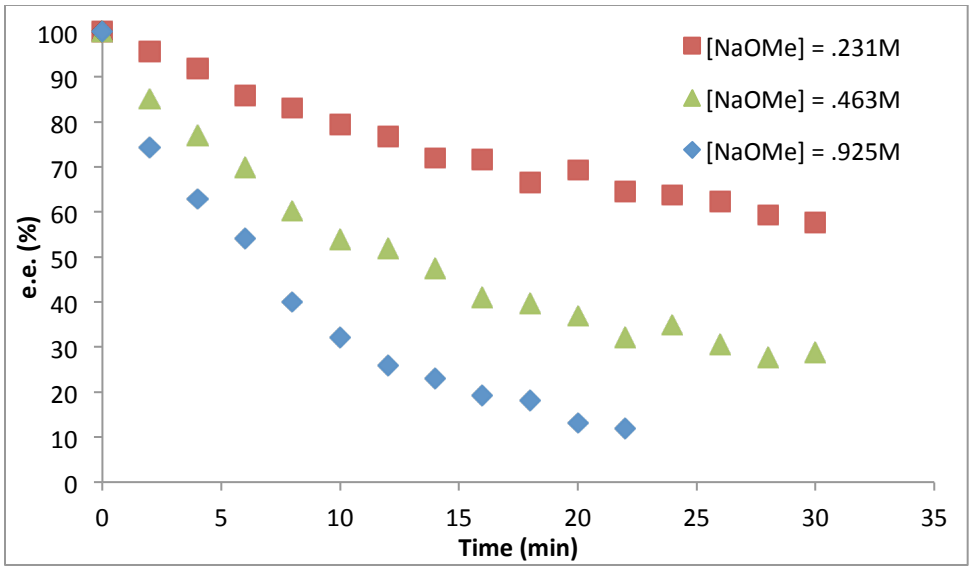

Figure 1-14: Rate of epimerization experiment done at room temperature (25°C). See Appendix V for experimental details.

Our curves do support the mechanism for epimerization. As the concentration of base increases, so does the rate of epimerization of Naproxen methyl ester. The above graphs show the rate of epimerization once base is added from enantiopure material to racemic at two different temperatures Experiments at two different temperatures were done to see the effect of rate versus temperature. Figure 1-13 shows the rate of epimerization at 45°C while the latter is done at room temperature. Rates increase at higher temperatures, as was expected. The solution of enantiopure naproxen methyl ester was set to stir at a moderate rate, allowing the system to become fully saturated. After the system has equilibrated, a known amount of sodium methoxide is added and epimerization begins. Over a period of an hour, the system is sampled and analyzed via HPLC-MS. Conditions and methods located in Appendix I for Naproxen methyl ester. For the higher base concentration at 45°C, the ee% returns to <1% within 55 minutes. For the lower base concentration, after 75 minutes the ee% is 3.5% and keeps decreasing slowly over the next 100 minutes.

From these data we can conclude that the rate of epimerization will be an issue for attrition enhanced deracemization. While the rate of crystallization varies considerable depending on the degree of supersaturation, in general, it occurs at approximately the same rate as we are observing for the epimerization. This would mean that if one enantiomer were to selectively be crystalized from solution, the depletion in concentration caused by this crystallization would not be immediately compensated by the solution phase racemization. The result is that since crystallization and

epimerization is occurring at the same rate the net mass movement we need to create one enantiomer to the other is hindered.

1.8 Separation system 1: Attrition Enhanced Deracemization using Two-Flasks

In the first method, one enantiomer is seeded in flask 2, which is held at a lower temperature, while the stockpile made up of a racemic mixture of conglomerate crystals is left in flask 1. The solution phase is saturated, but the temperature differential between flask 1 and 2 will lead to a net bias to dissolve material from flask 1 and accrete crystals in 2. As there is only a single enantiomer in flask 2 then we expect only the seeded enantiomer to grow over time.

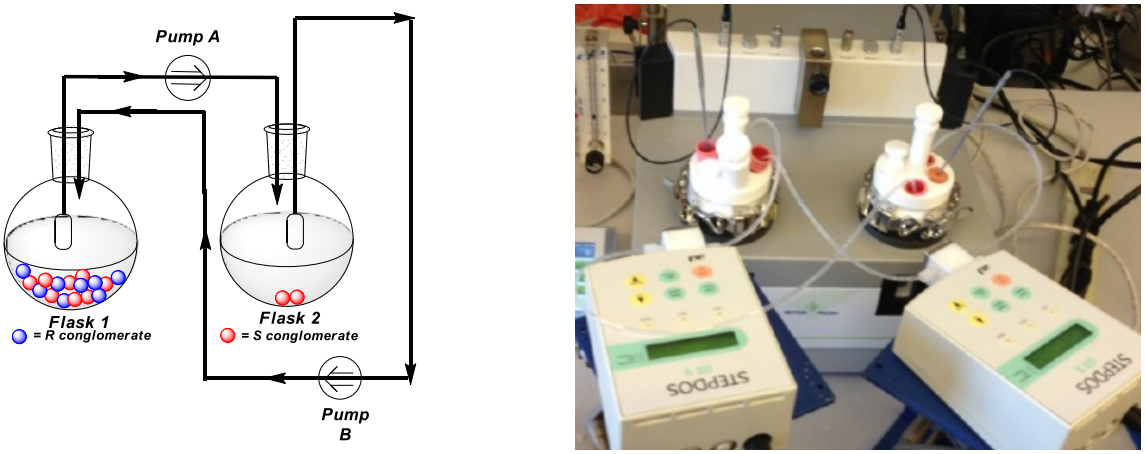

Figure 1-15: Schematic (left) and actual (right) set-up of the experiment for attrition enhanced deracemization using two flasks.

In the initial two flask system, a mother flask and a seed flask were used. Flask 1, the mother flask, was loaded with rac-**(1)** in MeOH to make a saturated solution with solid phase still left. The temperature was set so that it was at a slightly higher temperature (22°C) than flask 2 (20°C). The temperature was decided so that the temperature in flask 2 wouldn't be low enough to promote racemic primary/spontaneous nucleation but only just cool enough to allow the **S-(1)** to grow.

The system in flask 1 was stirred at a conservative rate and allowed to equilibrate at that set temperature. Then sufficient NaOMe was added to product a 0.5M solution. This allowed the naproxen methyl ester to epimerize in the solution phase. The system was then set to circulate until near equal amounts of the solution phase was in both flasks. After the system was seen

to be stable (no spontaneous nucleation was observed) flask 2 was seeded with 100 mg amount of S-(1). Over the course of 6 hours, crystallization of the S-(1) occurred in flask 2 with a full depletion of material in flask 1. After filtration 2g of enantiopure naproxen methyl ester was obtained stating from ~2g of racemic mixture.

This progress to enantiopurity was significantly faster than the result observed by Kaptein et al.(2009) who were only able to purify less than 1 gram over 5 days. We attribute this increase in efficiency to a lack of unproductive attrition. In the Kaptein example with only a single pot, grinding the crystal phase does not preferentially destroy only the unseeded enantiomer. This means that both the crystal that we are trying to isolate and the one we are converting from are ground down, preventing crystal ripening. While in the long run, solid phase e.e. does reach enantiopurity, it comes at the cost of many stochastic grinding events. By physically separating the destruction of the seed crystals (in flask 1) and the crystal growth (flask 2) we help to bias the system and favor net mass transfer to both the desired crystal and flask 2.

1.9 Separation system 2: Thermal ripening

We also expanded our study of naproxen methyl ester to explore the use a variable temperature gradients within one flask. A similar approach has been applied by Coquerel (2013), where a fast series of heating and cooling cycles was used to carry out deracemization. These temperature oscillations have a similar effect to a system as attrition with glass beads does by aiding rapid dissolution of particles. This method of thermal ripening is more practical and feasible when considering scale up onto a kilogram level.

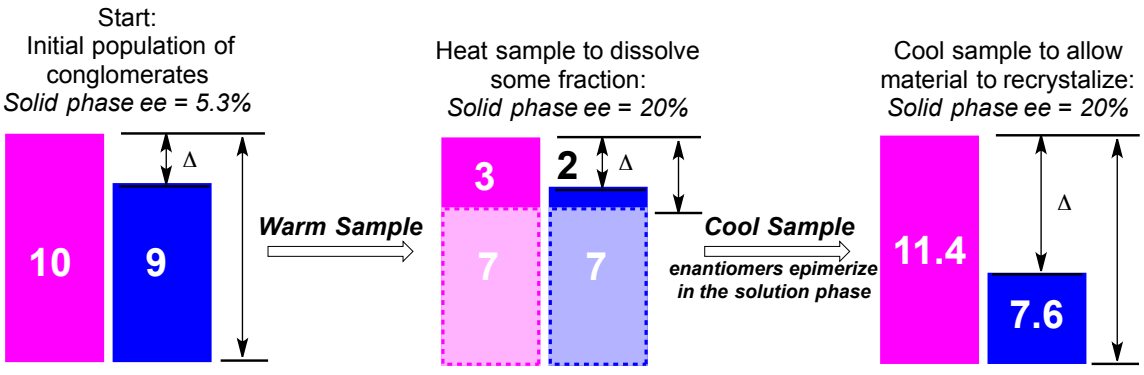

Figure1-16 : Theoretical progression of ee with temperature cycles.

The way in which a set of thermal cycles can lead to enantiopurificaion is shown in figure 1-16. Starting with an excess of one enantiomer in the solid phase, the solution is heated. Since the crystal is a conglomerate they will both have the same solubility so that equal amounts of both enantiomers undergo dissolution. This leads to a greater ratio between the two enantiomers in the solid phase, thus increasing the enantiomeric excess. Then on a slow cool down cycle, the ee% of the system will be retained, provided the rate of crystallization is fast compared to the rate of crystal growth. For example, if the system is heated up so that 7 grams of both enantiomers are dissolved, then the ratio left in the solid phase is 3:2 which would leave an enantiomeric excess of 20%. Over a period of heating and cooling cycles, the enantiomeric excess increases exponentially.

Using a one pot system, an equal amount of naproxen methyl ester was added with enough MeOH to make a saturated solution. One enantiomer is added to result in a small initial enantiomeric excess of approximately 10%. Then a NaOMe is added to the system to start epimerizing conditions. The Coquerel group discussed the potential industrial benefits of such a method as oscillating the temperature range in a rapidly epimerizing system (Coquerel et al., 2013). Our group conducted further background studies on the effects of amplitude and center point of temperature range, rate of cooling, and rate of epimerization to discover other important factors to consider upon implementing such a method, especially in a slow epimerizing system.

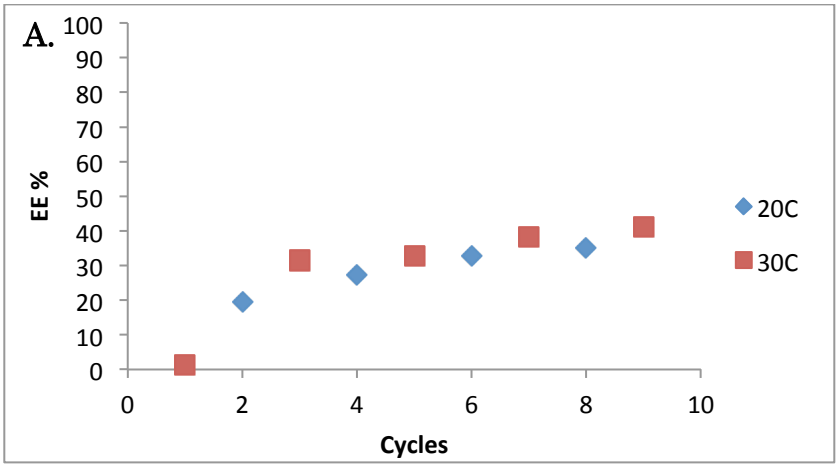

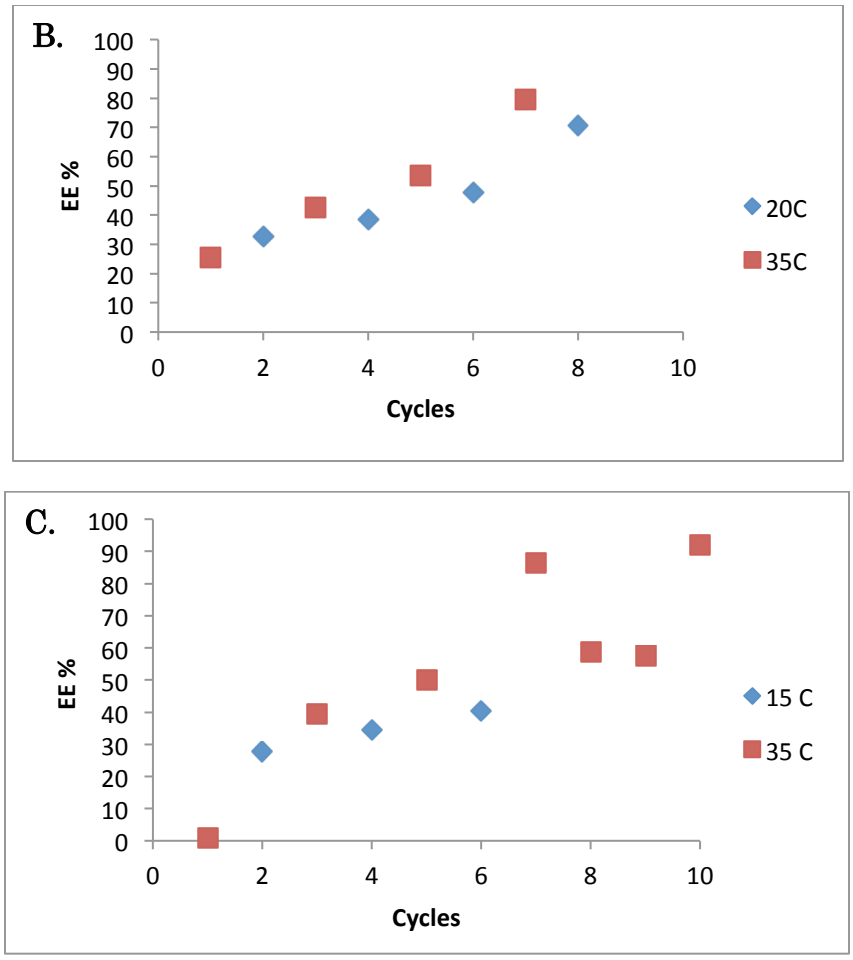

Figure 1-17 A-C: Evolution of ee% dependent on temperature range. The above plots are of cycles of heating and cooling showing the ee% after that specific cycle. A.) Temperature oscillations from 30°C to 20°C. B.) Temperature oscillations from 35°C to 20°C. C.) Temperature oscillations were from 35°C to 15°C. All runs were cooled at a rate of 0.1 K/min.

As far as efficiency of the thermal ripening system goes, a system that obtains a high ee% with merely a few temperature cycles is ideal. Knowing the solubility curve of naproxen methyl ester from a previous study, it was determined that the ideal temperature range to stay in was 15°C–35°C. This range was selected for a few reasons. The solution needs to be completely saturated at all times during the oscillations. Working at either extremes of the temperature spectrum-hot or cold- increases the chance of spontaneous nucleation of either enantiomer to occur. The experiments were from 30°C–20°C, 35°C–15°C, and 35°C–20°C. It was observed that ee% increased dramatically when more of the particles were dissolved around the upper temperature limit of 35°C. Along those lines, it makes sense that the lower

temperature limit of 15°C would enable more crystallization to occur. One worry was that the rate of crystallization would be too fast and coupled with slow epimerization cause racemic crystallization to occur. This is why a slow rate of cooling of 0.1 K/min or 0.2 K/min was determined to be the best choice with such a system.

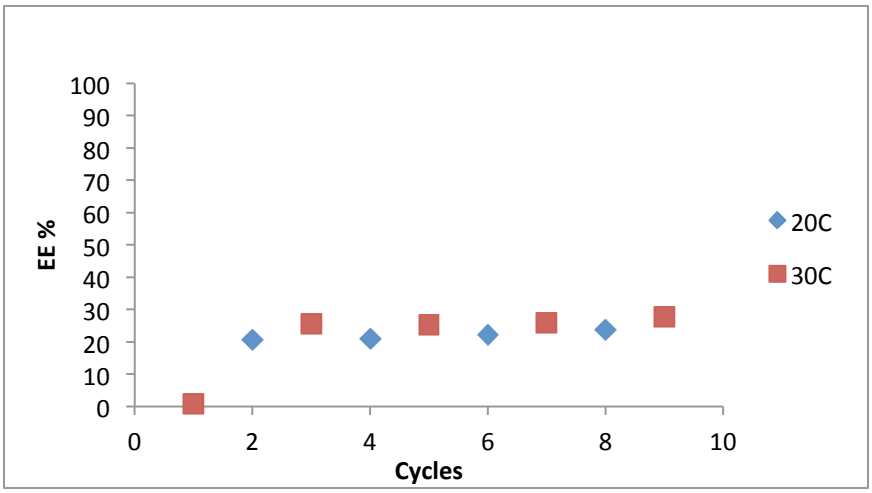

Figure 1-18: Evolution of ee% from oscillating temperature cycles of 30°C to 20°C at a faster rate of cooling, 0.4K/min.

1.10 Conclusions

In conclusion, the efficiency of the deracemization of naproxen methyl ester by a series of fast heating and cooling cycles was improved. This also is a much more practical method when scaled up, resulting in a better ee% and more product recovery. It was found that the rate of epimerization in a system such as this is an important factor controlling enantiopure crystallizations and, thus, should be considered and studied prior to designing the experiments. If the rate of epimerization is too slow and the cooling rate and temperature differential too wide, then both enantiomers will crystallize out of solution. On an industrial scale for naproxen methyl ester, attrition enhanced deracemization using two-flasks is a more efficient method for obtaining enantiopure material if one has seed crystals in order to promote nucleation. If this is not available, then thermal ripening may be the better option.

1.11 References

Blackmond, D.G., "Chiral Amnesia" as a Driving Force for Solid-Phase Homochirality, *Chem. Eur. J.* **2007**, 13, 3290 – 3295

Blackmond, D.G., Viedma, C., Ortiz, J.E., de Torres, T., Izumi, T., Evolution of Solid Phase Homochirality for a Proteinogenic Amino Acid, *J. Am. Chem. Soc.* **2008**, 130, 15274–15275

Coquerel, G., Suwannasang, K., Flood, A.E., Rougeot, C., Using Programmed Heating−Cooling Cycles with Racemization in Solution for Complete Symmetry Breaking of a Conglomerate Forming System, *Cryst. Growth Des.* **2013**, 13, 3498−3504

Gibbs, J.W., Collected works, Vol. I, *Thermodynamics*, Yale University Press, New Haven, **1948**

Hein, J.E., Cao, B.H., Viedma, C., Kellogg, R.M., Blackmond, D.G., Pasteur's Tweezers Revisited: On the Mechanism of Attrition-Enhanced Deracemization and Resolution of Chiral Conglomerate, *J. Am. Chem. Soc.,* **2012,** 134, 12629-12636.

Hein, J.E., Cao, B.H., van der Meijden, M.W., Leeman, M.L., Kellogg, R.M., Resolution of Omeprazole Using Coupled Preferential Crystallization: Efficient Separation of a Nonracemizable Conglomerate Salt under Near-Equilibrium Conditions, *Org. Process Res. Dev.,* **2013**, 17, 946−950

IUPAC, Compendium of Chemical Terminology, 2nd ed. (the "Gold Book"), Compiled by A.D McNaught and A. Wilkinson, Blackwell Scientific Publications, Oxford, **1997**.

Jacques, J., Collet, A., Wilen, S.H., *Enantiomers, Racemates and Resolutions*, Malabar, Fla: Krieger, 1994

Kaptein, B., Noorduin, W.L., Meekes, H., van Enckevort, W.J.P, Kellogg, R.M, Vlieg E., Fast Attrition-Enhanced Deracemization of Naproxen by a Gradual In Situ Feed, *Angew. Chem. Int. Ed.* **2009**, 48, 4581 –4583

Kunz, G.F., "The Life and Work of Haüy." American Mineralogist. Volume 3, number 6, **1918**, Pages 61–89

Lakhtakia, A. (ed.), *Selected Papers on Natural Optical Activity*, **1990,** *(SPIE Milestone Volume 15)*. SPIE

Leitereg, T.J., Guadagni, D.G., Harris, J., Mon, T.R., Teranishi, R., Chemical and sensory data supporting the difference between the odors of the enantiomeric carvones, *J. Agric. Food Chem.* **1971,** 19, (4): 785.

Lorenz, H., Polenske, D., Seidel-Morgenstern, A., Application of Preferential Crystallization to Resolve Racemic Compounds in a Hybrid Process, *Chirality*, **2006,** 18, 828-840.

Levilain, G., Coquerel, G., Pitfalls and Rewards of Preferential Crystallization, *Cryst. Eng. Comm.*, **2010,** 12, 1983-1992.

Liesegang, R. E., Z. Phys. Chem. Stoechiom. Verwandtschaftsl., **1911**, 75, 374

Noorduin, W.L., van der Asdonk P., Bode A.A., Meekes H., van Enckevort W.J., Vlieg E., Kaptein B., van der Meijden M., Kellogg R.M., Deroover G., Scaling up Attrition-enhanced Deracemization by use of an Industrial Bead Mill in a Route to Clopidogrel (Plavix), *Org. Process Res. Dev.*, **2010,** 14, 908–911

Ostwald, W., *Lehrbuch der Allgemeinen Chemie*, Vol. 2, Part 1, Engelmann, Leipzig, **1896**.

Pasteur, L., Mémoire sur la relation qui peut exister entre la forme cristalline et la composition chimique, et sur la cause de la polarisation rotatoire, *C.R. Hebd. Seances Acad. Sci.* **1848**, 26, 535-538

Viedma, C. Experimental evidence of chiral symmetry breaking incrystallization from primary nucleation, *Journal of Crystal Growth*, **2004,** 261, 118–121,

Viedma, C., Chiral Symmetry Breaking During Crystallization: Complete Chiral Purity Induced by Nonlinear Autocatalysis and Recycling, *Phy.Rev.Lett.,* **2005**, 94, 065504

Chapter 2:

Importance of Homochiral vs. Heterochiral Crystal Solubility in Method Development of Asymmetric Reactions: Approaches to a New Hypoxia Inducible Factor Inhibitor

Abstract:

Asymmetric synthesis was employed to generate a singled enantiomer of a key intermediate needed to access a new class of hypoxia inducible factor inhibitor. The key challenge was to identify conditions to access the target molecule as a single enantiomer. However, challenges stemming from solubility differences in the product have led to confusing and irreproducible results. By studying the solid phase behavior of the enantiopure and racemic product it was revealed that the homochiral crystal is many orders of magnitude more soluble than the heterochiral crystal. In addition, the heterochiral crystal was found to adopt at least two different polymorphic phases. This behavior is partly responsible for the difficulty optimizing and controlling the enantioselectivity of the reaction.

Introduction

2.1 Hypoxia Inducible Factors

Hypoxia is a condition where the body or a certain region of the body is deprived of oxygen. To protect itself from intercellular and systemic damage, the body produces hypoxia inducible factor (HIF) to minimize the effects of hypoxic injury (Ratcliffe et al., 2008). HIF activity promotes angiogenesis, which is the growing of new blood vessels from current ones. The majority of advanced stage tumors contains areas of decreased oxygen availability, and thus is a high region of HIF activity (Semenza, 2007). This is normal for cell development but there is no way for the body to differentiate HIF for normal healthy cell development versus a cancer tumor. Thus, a way to inhibit certain HIFs from being produced is needed. HIF inhibitors are members of bHLH/PAS family of transcription factors and have significant possible implications in cancer research by causing the gene transcription of certain cancer cells to be inactive (Semenza, 2012). The molecule of interest is classified as a HIF-2α inhibitor. The cavity within the HIF-2 α protein is of particular interest due to its relatively large size of 290 $Å^3$ (Gardner et al., 2009). Due to the preformed space within the protein, the question was raised as to whether or not a small molecule could fit inside the preformed cavity and possibly cause any conformational change to the protein and thus, deactivating it.

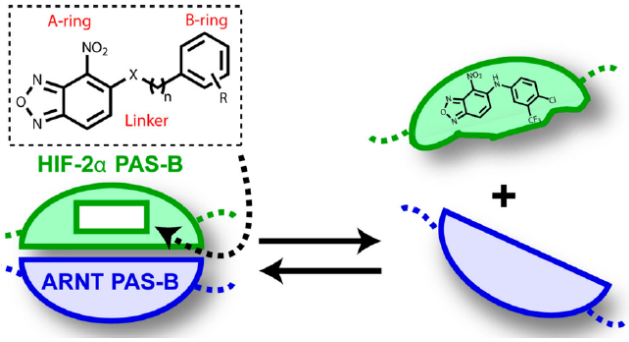

Figure 2-1: A schematic representing insertion of a small molecule into the internal cavity of HIF-2α PAS-B. This destabilizes the HIF-2α – ARNT complex where gene transcription can no longer occur (Rogers et al., 2013)

2.1.1 HIF-2α Inhibitors

Currently there are two types of HIF-2α inhibitors, scaffold I and scaffold II The potency of scaffold I is much greater than the current scaffold II molecules.

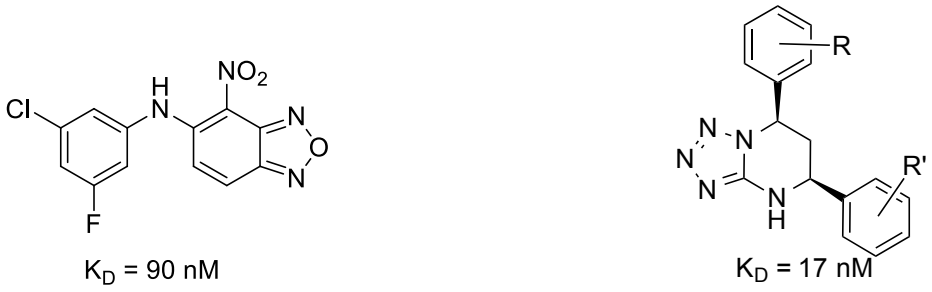

Scaffold I HIF-2α inhibitor

Scaffold II HIF-2α inhibitor

Figure 2-2: Examples of Scaffold I and II HIF-2α inhibitors and the corresponding potency of the molecule. (Rogers et al., 2013)

Current efforts in the Tambar lab at the University of Texas Southwestern Medical Center, are focused not only at increasing the potency of the Scaffold II HIF-2α inhibitors but also, more efficient production of these molecules. Preliminary results from the Tambar lab have shown that of the possible stereoisomers of a model compound from the Scaffold II class, only the (5*S*,7*R*) enantiomer is highly biologically active.

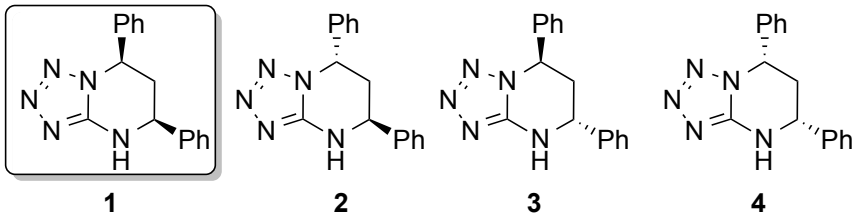

Figure 2-3: Possible enantiomers with **1** as the desired HIF-2α inhibitor.

Thus the challenge becomes to obtain compound **1** via some form of asymmetric synthesis pathway. This compound could be obtained by way of diasteroselctive reduction of **5**, which would in turn be generated by coupling aminotetrazole **6** and chalcone **7**. Preliminary experiments by Prof. Tambar's group has shown that reduction from **5** to **1** is completely diastereoselective, requiring only $NaBH_4$ to obtain the desired product. Thus, being able to obtain the intermediate **5** as a single enantiomer would allow the desired scaffold to be created as a single enantiomer. The primary focuses of this chapter are of polymorph formation, control of the reaction and enantiopurification of the molecule of interest.

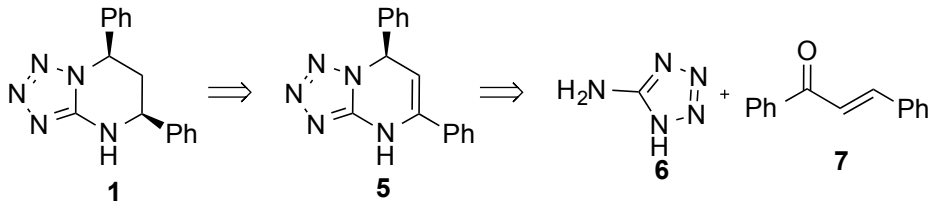

Figure 2-4: Retrosynthetic approach of the desired molecule.

2.2 Polymorphism and Differences in Heterochiral and Homochiral Crystal Structures

Polymorphs occur when the same chemical compound forms different crystal structures and can be distinguished via X-ray crystallography or X-ray Powder Diffraction. Polymorphism is an important topic to be aware of because those crystal structures exhibit different physical and chemical properties, such as solubility, melting point, density, chemical stability. (Blatter & von Raumer, 2006) Polymorphs also have different stabilities due to the intermolecular and intramolecular interactions because of differing crystal structure.

Figure 2-5 : Schematic of polymorphs.

Polymorph formation is very common in small organic molecules with low molecular weights, generally less than 600 g/mols. (Lipinkski et al., 2001; Griesser and Stowell, 2003) Amorphous forms, solvates, salts, and co-crystals are other crystalline forms that can occur which will affect the behavior of the molecules but the primary focus will be on general polymorphs formation and the issues that will occur. Polymorphs have different free energies and thus differing stabilities due to the forces within and around the molecule. Thus, the most stable polymorph has the lowest energy. The other polymorph(s), the metastable polymorphs, are thermodynamically unstable but over time can transform into a more stable polymorph. (Grant and Lohani, 2006)

Aside from simple polymorphs, involving different arrangements of the same molecule, chiral molecules also have two other possible variations in their crystal form. Heterochiral (racemate) crystals are structures containing both enantiomers while a homochiral (conglomerate) crystal contains just a single enantiomer within its unit cell. Though the structures only differ by their crystal arrangement, they may possess extreme differences in

solubilities. The solubility differences are due to differing hydrogen bonds and van der Waals interactions resulting in different free energies for each possible isoform.

2.3 Solubility Differences in Heterochiral and Homochiral Systems

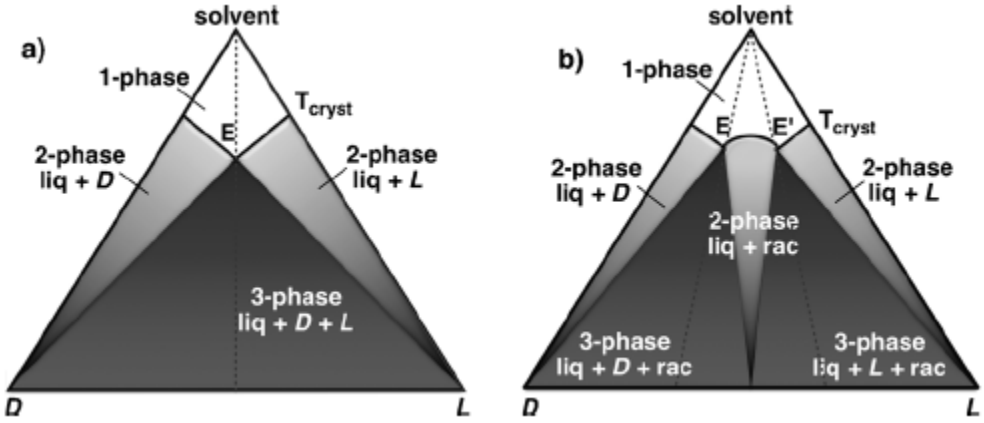

Figure 2-6: Ternary phase diagrams for a chiral compound of (a) conglomerate forming crystals and (b) racemate forming crystals. Reprinted from (Johnson et al., 2014)

This difference in solubility can be harnessed to do effective crystallization methods. With knowledge of the solubility of both crystal phases, a successful enantiomeric separation can occur. Homochiral systems have a ternary phase diagram (a) only involving the single enantiomer and the solution phase, while heterochiral systems (b) have a ternary phase diagram with the racemate crystal, solution phase, and the single enantiomer crystal. The solubility difference between heterochiral and homochiral systems can be measured experimentally by taking the enantiomeric excess (*ee%)* of a saturated solution phase. The solution phase of a homochiral system will always have an *ee%* = 0 because there is an equal amount of both D and L crystals dissolved. A saturated solution of a heterochiral system will contain an *ee%* because of the difference in solubility of the conglomerate and racemate crystals.

Results and Discussion

2.4 Hypotheses

Because of the possible pharmaceutical benefits of the Scaffold II HIF-2α Inhibitor, efficient production and synthesis of the active enantiomer is needed. It was initially thought that the enantiopurification of the target molecule, **5,** would be easily achievable via a two pot attrition enhanced deracemization method similar to the first chapter. However, the molecule did not crystalize as a stable conglomerate and no easy method for chemical racemization could be identified. Therefore, the research focus shifted to further understand the mechanism and the crystal formation of the molecule including the formation of possible polymorphs.

2.5 Preliminary Results and Mechanistic Hypotheses

There are two different mechanistic routes by which the target molecule **5** could be synthesized, along with several non-productive side products. Path 1 is initiated when the secondary nitrogen of **6** acts as a nucleophile and attacks the carbon at the β position of **7** to form the enolate intermediate **8.** This intermediate undergoes proton exchange to give **9.** Under acidic conditions, the carbonyl is reformed giving **10**. Then a second nucleophilic attack occurs in which the primary nitrogen on **11** adds to the carbonyl carbon to close the ring. A condensation reaction in which water is expelled from **13** is the final step to get to the product **5.**

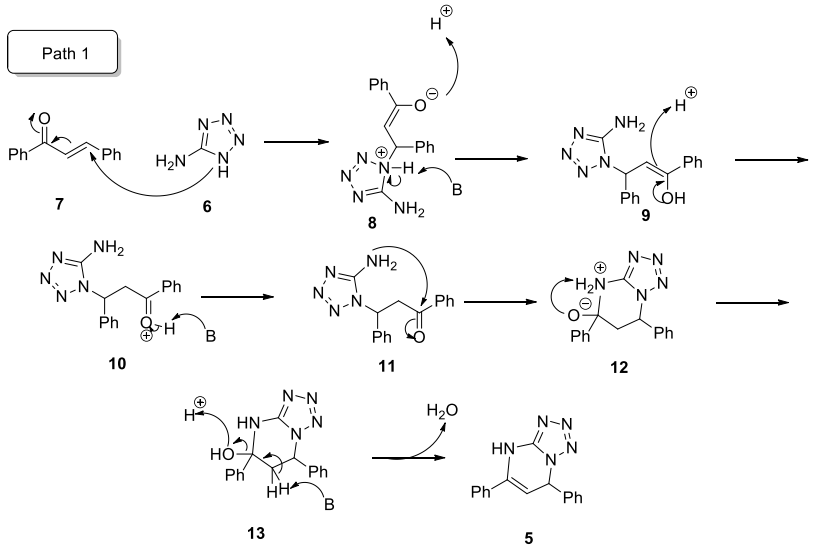

Figure 2-7: Path 1 mechanism for the formation of 5,7-diphenyl-4,7-dihydrotetrazolo[1,5-a]pyrimidine. This path proceeds first via an α, β Michael type addition and imine formation ring closure.

Alternatively path 2 proceeds via a nucleophilic attack by the primary nitrogen on **6** to the carbonyl carbon on **7** to form **14** which then undergoes condensation **15** to expel a water from the molecule forming the imine **16.** The final ring closure step is a nucleophilic attack at the β position of the imine to give **5**.

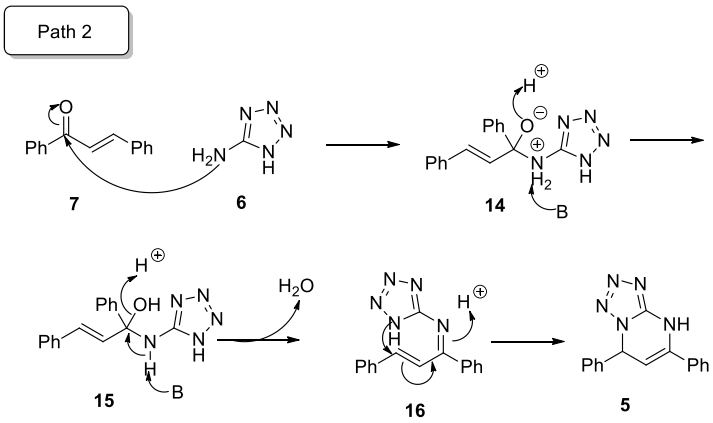

Figure 2-8: Path 2 mechanism for the formation of 5,7-diphenyl-4,7-dihydrotetrazolo[1,5-a]pyrimidine. This path would proceed first by imine formation then an α, β Michael type addition.

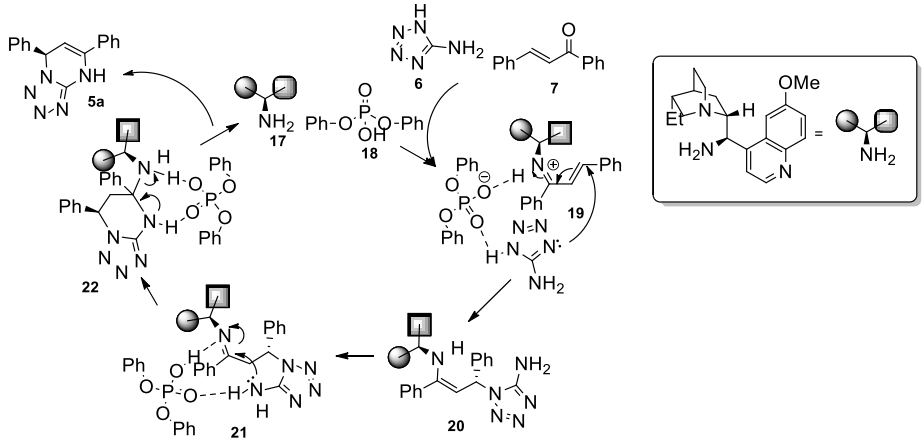

Figure 2-9: Proposed mechanism for the enantioselective catalytic reaction.

In the enantioselective reaction a catalyst **17** and a phosphoric acid co-catalyst **18** are used. The primary nitrogen on **17** condenses with **7** forming an imine while **18** forms a complex with both the secondary nitrogen of **6** and the newly formed imine. This aids in the nucleophilicity of the secondary nitrogen of **6** leading to attack at the carbon β to the imine as shown in **19**. The enamine form, **20**, tautomerizes to **21** and re-forming a complex with the phosphoric acid co-catalyst to aid in a second nucleophilic attack by the

primary nitrogen towards the carbon of the enamine, closing the ring to give **22**. The catalyst is recycled and **5a** is formed.

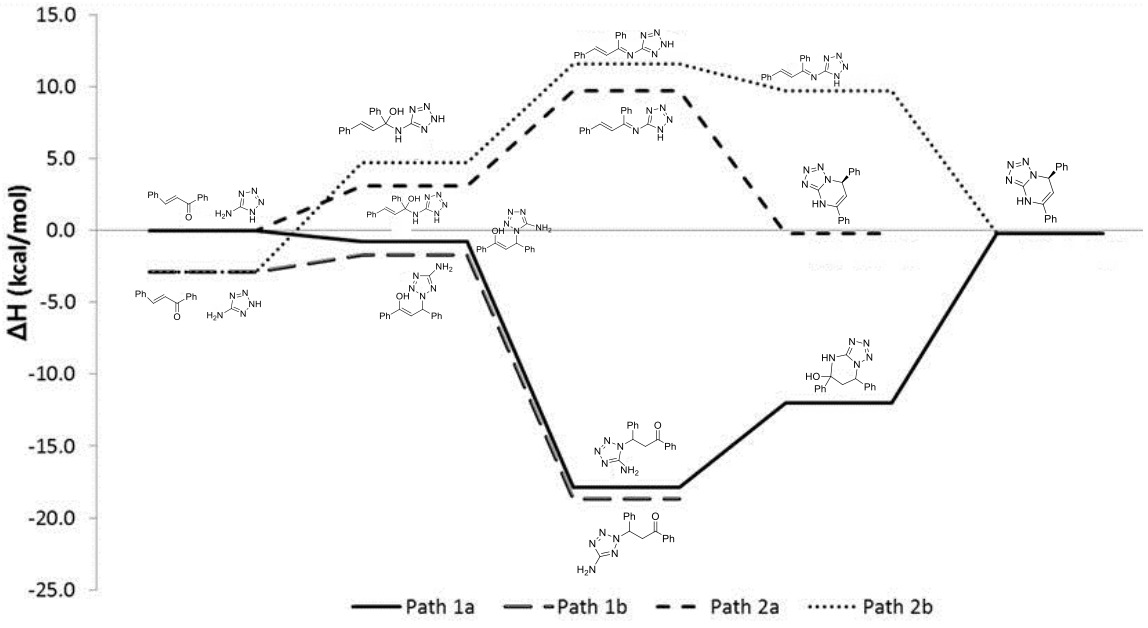

Figure 2-10: Calculated energies of possible pathways and side products.

The results of the calculations, run by the Johnson lab, are shown above. Energies of all the intermediates and the different pathways were calculated. Path 1a was determined to be the most energetically favorable route. Gas-phase geometry optimizations and frequency calculations were performed in Gaussian 09 using BLYP/6-31G* with XDM (Otero de la Roza, 2013). All ΔH values include ZPVE corrections, and are reported in kcal/mol.

Although path 1 is the most energetically favored route according to the calculations above, there seems to be a slight problem due to the need for an input of energy in the middle of the reaction. Path 2 seems to be the least likely pathway due to the relatively high energies of the intermediates formed.

2.6 Reaction Screening

In an attempt to improve the observed enantioselectivty, reaction parameters were varied. Screening reaction conditions lead to random and irreproducible results. In many cases, systematic variation of parameters such as solvent, temperature, water content and acid added did not produce any discernable trends. One particular point of note was that in all cases the

reaction started as heterogeneous system, then on heating all solids dissolved. After some period of time, a new solid appears. On isolation this was identified as the product, but more importantly, this solid was found to be racemic. Our approach was to allow the reaction to progress and analyze samples at particular time points by chiral HPLC.

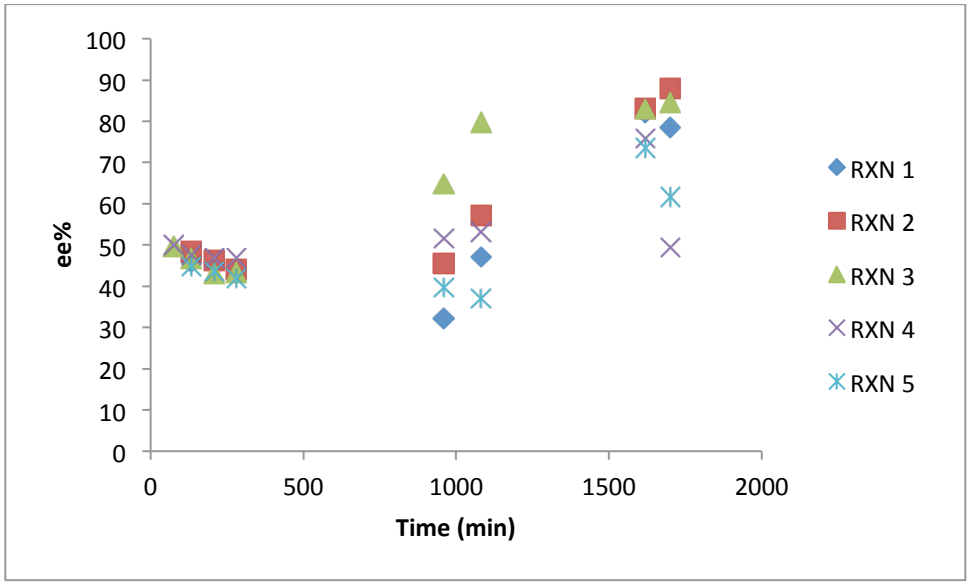

Figure 2-11: Normal protocol was followed of the catalytic enantioselective synthesis and an internal standard was added. Five reaction vials were set up in parallel and sampled over the course of 1700 minutes. See Appendix II C for experimental details.

In figure 2-11, the ee measured in all five reaction vials are relatively the same for the first 280 minutes. The ee distribution of the five reaction vials increases over the rest of the time course. Another noticable characteristic is seen around 1000 minutes where reaction 3 has the highest ee but is beat out by reaction 2 a few hours later. The trend around 1000 minutes would lead us to believe that the ee for reaction 3 would keep increasing towards 100% ee. Instead, the ee seems to top out around 82% ee. Reaction 2, on the other hand, sees a steady increase in ee from 900 minutes to the end of the sampling time. The variation we are seeing between these reactions is possibly because of a major solubility differences between crystal forms present in the solution- racemate, single enantiomer, and other isoforms. Several reaction batches were sampled and the evolution of ee over time was found. Most batches had irreproducible ee that seemed to fluctuate over the course of the reaction sampling.

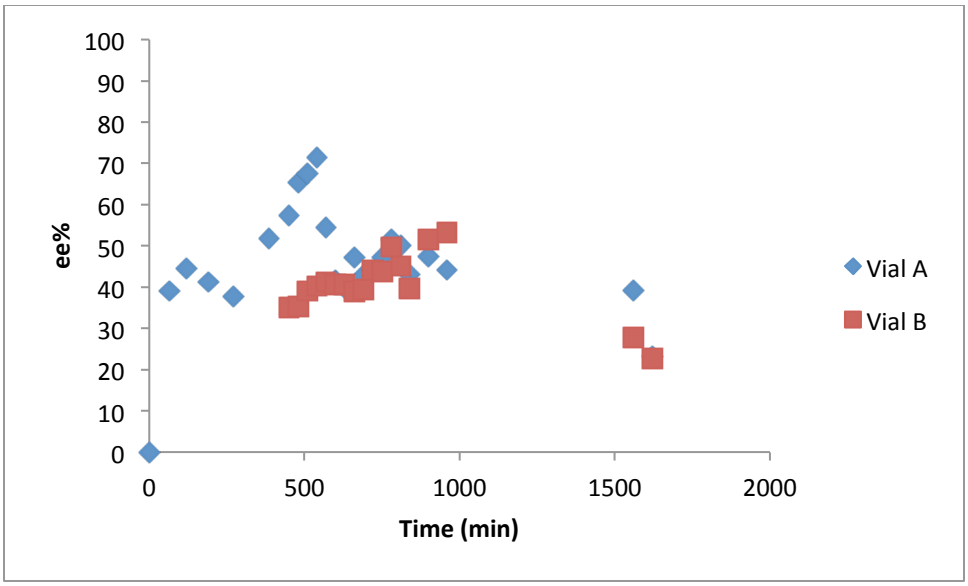

Figure 2-12: No deviations from the catalytic enantioselective synthesis. Two identical reactions were set up at the same start time. Vial A was sampled from the beginning at all time points while Vial B was left alone until 450 minutes into the reaction. An internal standard was also used in the above reactions.

The experiment in figure 2-12 was similar in concept to figure 2-11. The only difference was that one vial was left alone for the first half of the reaction to see if sampling had an effect on the evolution of ee. In vial A, the ee seems to evolve as expected until a sudden drop around 570 minutes where it seems to level out around 45 ee%. Vial B was left undisturbed until its first sample timepoint at 450 minutes. The ee for vial B slowly increased until it dropped sharply later on similarly to Vial A.

From figures 2-11 and 2-12, it is obvious that the ee is irreproducible which presents a major challenge to reaction optimization and further enantiopurification studies. This could be due to solubility of different isoforms forming in the reactions.

2.7 Solubility Confirmed by Gravimetric Analysis

Gravimetric analysis is a very accurate method for obtaining solubilities and contains low error because there is no need for a standard or calibration of instruments.

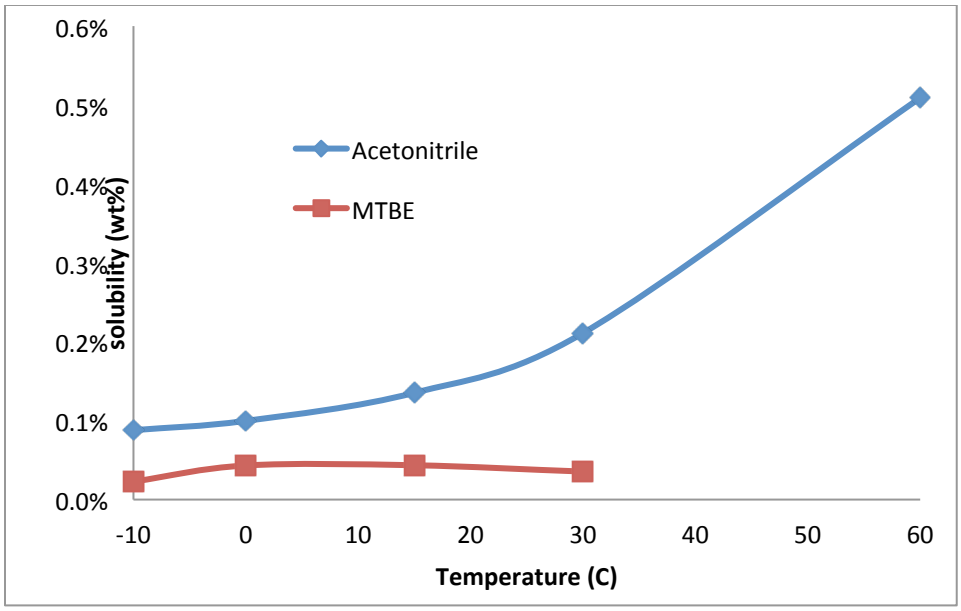

Figure 2-13: Solubility curve of the rac-Tetrazole, **5**, in Acetonitrile and MTBE by gravimetric analysis. See Appendix IV for details.

The solubility of **5** was measured in two different solvents, MTBE and Acetonitrile. MTBE proved to be a terrible solvent for the rac-Tetrazole with the solubility never rising above 0.05%. Acetonitrile was not much better. When the solution was heated up to 60°C the solubility was merely 0.5 wt%. From this, we were able to determine that the racemate crystal is relatively insoluble which is problematic if there seems to be little control over the ee% as seen in the previous section.

Another method of obtaining a solubility curve is by using a ReactIR which is an IR probe that can be placed in a vessel and monitor IR response in real time. First, known amounts of tetrazole are added to a certain amount of solvent until a saturated solution is obtained. Then the system is heated up in small temperature increments to obtain a solubility curve. There are a few problems with this method of obtaining a solubility curve. The first is that IR absorbance is small or reversed when working with a relatively insoluble compound such as the tetrazole. This can lead to false results of reverse solubility behavior. Though there are some disadvantages for using the ReactIR in all circumstances for solubility measurements, the ReactIR is efficient and reliable for those compounds with higher solubility.

2.8 Polymorph Formation

Upon synthesizing different batches, the tetrozolo compound exhibited quite differing physical characteristics: clear, rhomboid shaped crystals,

clumpy white powder, and fine granules. No deviations from the procedure were made during any of the above syntheses. All batches of the were analyzed by XRPD (x-ray powder diffraction) for quality. Below is the XRPD for three separate batches of racemic tetrazole and upon first glance it is obvious that one of the batches has a different diffraction pattern.

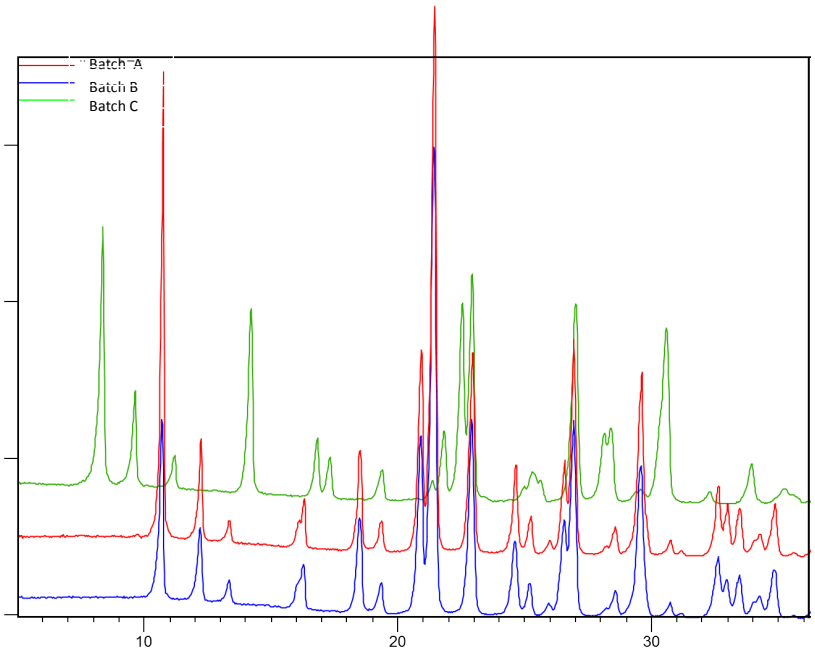

Figure 2-14: XRPD of several batches of racemic tetrazole, **5**. Batch C clearly has a different scattering pattern that the other batches and is concluded to be a polymorph. XPRD analyses were performed using a PANalytical X'Pert PRO θ/θ diffractometer equipped with a X'Celerator detector and X-ray beam consisted of the Co Kα1 radiation (λ=1.7890 Å). Routine XRPD analyses were performed with a step of 0.02° (2θ) between 5 and 30° 2θ.

From the above XRPD pattern, we know that the tetrazolo compound can form polymorphs. This will present a challenge to implementing a crystallization method because of the possibility of an undesired polymorph crystallizing instead of the desired polymorph. The possibility of polymorph formation occurring will affect the solubility as well. Single crystal X-ray was taken of Batch A and thus, confirms formation of the racemate crystal. Batch C is assumed to be a metastable polymorph.

2.9 Difference in Solubility of Heterochiral and Homochiral Crystal Phases

Individual X-ray analysis was carried out on crystals recorded from both racemic mixtures and enantiopure samples. (See appendix for full structure report). This allowed us to obtain the crystal packing for both the conglomerate and racemate crystal phase for the tetrazole product. DFT can

then be used to predict that the solubility difference between the two different crystal forms. These calculations confirm that the racemate crystal is more stable by 5.82 kcal/mol, leading to a very large predicted solubility difference. In fact, the solution phase of a system containing only a small excess of one enantiomer is predicted to be enantiopure.

2.10 Projected Strategy

The solubility of the racemate crystal was frustratingly low to carry out an enantiopurification method as we had originally hoped. Due to the difference in the solubility of the racemate crystal and the single enantiomer, it seems to be possible to harness this vast difference in solubility in our favor to obtain enantiopure material. We were able to get near enantiopure material by running the catalytic synthesis and then purifying the material on a silica gel column. Though this method does increase the ee, the yield of material is rather low. This method will work since the racemic compound has very low solubility in organic solvents, whereas, the conglomerate compound is soluble in most polar organic solvents.

Trial	ee%
1	90.46
2	73.11
3	95.28
4	100.00

Table 2-1: These ee% values were obtained after column chromatography on achiral silica gel using a mobile phase of 1:1 hexanes and ethyl acetate. Values shows are from multiple runs using the same conditions

2.11 Conclusions

In conclusion, we were able to isolate and crystallize two different isoforms of the racemate. We also obtained single crystal X-ray of both the homochiral and heterochiral crystals. There is a vast difference in the solubility of the racemate and the conglomerate crystal forms of the molecule of interest which needs to be considered when doing any asymmetric catalytic method development. Overall, what seemed at first to be a frustrating task due to the relatively insoluble nature of the racemate crystal can indeed be leveraged in our favor allowing for the isolation of enantiopure material.

2.12 References

Becke, A.D., Johnson, E.R., *J. Chem. Phy.* **2005,**122, 154104

Blatter, F., Fritz, B., von Raumer, M. "Relevance of Solid-State Properties for Pharmaceutical Products". In *Polymorphism in the Pharmaceutical Industry*. Hilfiker, R., Ed.; Wiley-VCH: Weinheim, **2006**; pp 1.

Grant, D.J.W., Lohani, S., "Thermodynamics of Polymorphs". In *Polymorphism in the Pharmaceutical Industry*. Hilfiker, R.; Wiley-VCH: Weinheim, **2006**; pp 21

Griesser, Ulrich J., Stowell, J.G., In *Pharmaceutical Analysis*; Lee, David C., Webb, Michael L., Eds; Blackwell Publishing Ltd.: Oxford, **2003.**

Johnson, E.R., Otero-de-la-Roza, A., Cao, B.H., Price, I.K., Hein, J.E., Predicting the Relative Solubilities of Racemic and Enantiopure Crystals by Density-Functional Theory, *Angew. Chem. Int. Ed.* **2014**, 53, 7879-7882.

Key, J., Scheuermann, T.H., Anderson, P.C., Daggett, V., Gardner, K.H., Principles of Ligand Binding within a Completely Buried Cavity in HIF 2α PAS-B., *Journal of the American Chemical Society,* **2009**, 131(48), 17647-17654.

Lipinski, C.A., Lombarda, F., Dominy, B.W., Feeney, P.J., Experimental and Computational Approaches to Estimate Solubility and Permeability in Drug Discovery and Development Settings, *Adv. Drug. Deliv. Rev.,* **2001**, 46, 3-26.

Otero de la Roza, A and Johnson, E. R. Non-Covalent Interactions and Thermochemistry using XDM-Corrected Hybrid and Range-Separated Hybrid Density Functionals. J. Chem. Phys. 138, 204109 (2013)

Ratcliffe, P.J., Smith, T.G., Robbins, P.A., The Human Side of Hypoxia Inducible Factor, *British Journal of Haematology*, **2008**, 141, 325-334.

Rogers, J.L, Bayeh, L., Scheuermann, T.H., Longgood, J., Key, J., Naidoo, J., Melito, L., Shorkri, C., Frantz, D.E., Bruick, R.K., Gardner, K.H., MacMillan, J.B., Tambar, U.K., Development of Inhibitors of the PAS-B Domain of the HIF-2α Transcription Factor, *J. Med. Chem.*, **2013**, 56(4), 1739-1747.

Semenza, G.L., Evaluation of HIF-1 Inhibitors as Anticancer Agents, *Drug Discovery Today*, **2007**, 12, 853-859.

Semenza, G.L., Hypoxia-Inducible Factors: Mediators of Cancer Progression and Targets for Cancer Therapy. *Trends Pharmacol Sci.,* 2012, 33(4), 207-214.

.

Appendix I

HPLC/MS Conditions

LC samples were analyzed on by HPLC/MS on an Agilent 1260 Infinity using one of the following methods.

For all compounds:

> Agilent Poroshell, 120 EC-C18, 2.1 x 30 mm, 2.7 micron column, Temperature = 25°C, Solvent A = water, 0.05% TFA; Solvent B = acetonitrile, 0.05% TFA; Flow Rate = 0.6 mL/min; Starting Conditions = 95% A, 5% B; 0 – 0.1 min 15% B; 0.1 min – 7 min 100% B.

For Naproxen:

> Chiralcel® OJ-RH, 4.6 mm x 150 mmL, 5 micron, Temperature = 25°C, Solvent A = water, 0.05% TFA; Solvent B = acetonitrile, 0.05% TFA; Flow Rate = 0.500 mL/min; Starting Conditions = 30% A, 70% B; Run Time = 12 min.

For Tetrazole compounds:

> Chiralpak® AS-RH, 4.6 mm x 150 mmL, 5 micron, Temperature = 25°C, Solvent A = water, 0.05% TFA; Solvent B = acetonitrile, 0.05% TFA; Flow Rate = 0.650 mL/min; Starting Conditions = 45% A, 55% B; 0.1- 13 min 85% B; 13.1-14 min 100% B.

Appendix II

A.

Synthesis of methyl 2-(6-methoxynaphthalen-2-yl)propanoate

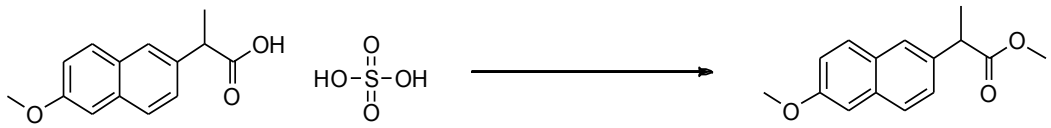

To a methanol solution of (RS)-2-(6-methoxynaphthalen-2-yl)propanoic acid add concentrated H_2SO_4 and stir reaction mixture overnight. Rotavap off most of the MeOH. Then dilute with CH_2Cl_2 (ca. 50 mL) and wash with saturated $NaHCO_3$ aqueous solution and dry over sodium sulfate. Rotavap off DCM.

B.

Synthesis of (R)-5,7-diphenyl-4,7-dihydrotetrazolo[1,5-a]pyrimidine

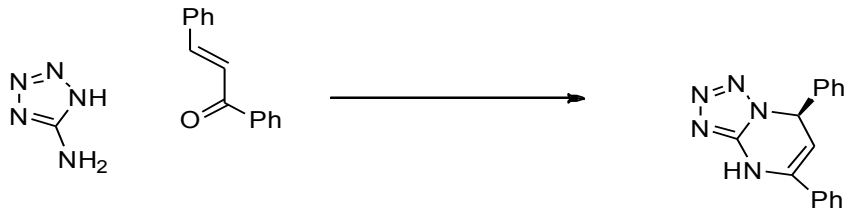

Add 1H-tetrazol-5-amine (.99983 g, 11.75 mmol) to DMF (Volume: 1.959 ml, 6 M) in an oven dried vial, then add (E)-chalcone (2.69 g, 12.93 mmol) to the vial. Allow to heat up to 150°C and stir. This batch was stirred overnight (~20 hours). Then while still heating (if taken off the heat, the stir bar will get stuck once everything solidifies), dilute with toluene (0.4M added ~0.4 mL) and stir for 2 more hours. Solid precipitate is collected via vacuum filtration and placed on high vacuum (reduced pressure) until dry. Rinse with toluene to get unreacted chalcone off product.

C.

Catalytic synthesis of (R)-5,7-diphenyl-4,7-dihydrotetrazolo[1,5-a]pyrimidine

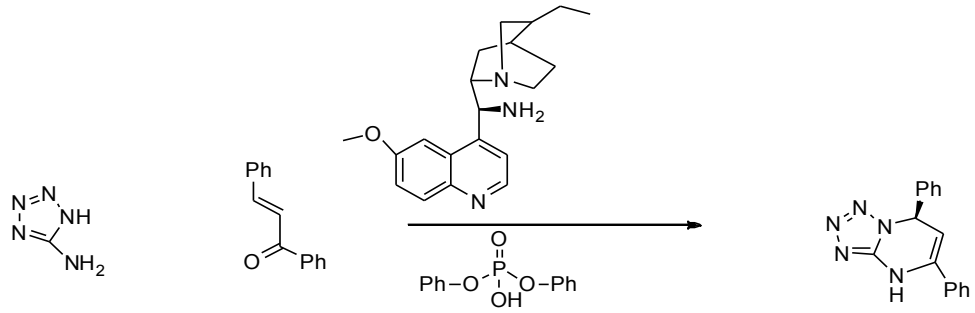

A flame-dried vial with a stir bar was charged with the cinchona alkaloid catalyst(1S)-((1S,2S,4S)-5-ethylquinuclidin-2-yl)(6-methoxyquinolin-4-yl)methanamine (0.191 g, 0.588 mmol), diphenyl hydrogen phosphate (0.294 g, 1.176 mmol), 1H-tetrazol-5-amine (.5 g, 5.88 mmol), and (E)-chalcone (1.224 g, 5.88 mmol). The vial was evacuated and purged with N_2 (g) followed by addition of anhydrous MeCN (1 mL). The vial was tightly sealed using a non-septa screw cap and the reaction was heated to 80 °C while stirring overnight. The mixture was then cooled to room temperature and diluted with ~2 mL trichloroethanol. The mixture was concentrated under reduced pressure (rotovap) until the MeCN was removed. The reaction was then made nearly homogenous with the addition of CH_2Cl_2 (~2 mL) and loaded onto an achiral silica gel column. Eluted with 1:1 hexanes: ethyl acetate.

Appendix III

Solubility Measurement using React IR

1.) Prepare a vial with a known amount of solvent.

2.) Prep the IR probe and blank the system in the solvent as is protocol.

3.) At room temperature, start adding in known amounts of the compound of interest. Allow the IR signal to equilibrate before adding again.

4.) Once a saturated solution is obtained, add excess.

5.) Increase the temperature in small amounts (about 5 to 10 degrees) and allow the IR signal to equilibrate before increasing the temperature again. Repeat this until the desired temperature/solubility measurement is obtained or IR signal won't respond to change (i.e. all dissolution has occurred)

6.) From these measurements one can find the IR response to dose amounts of compound and IR response to temperature and thus, obtain a solubility curve.

Appendix IV

Solubility Measurement using Gravimetric Method

1.) Prepare a saturated solution of compound of interest in the solvent and stir overnight (at least) at a constant temperature.

2.) Stop the stirring, let solid settle and decant.

3.) Weigh a vial. This is mass 1.

4.) Take saturated liquid up in a syringe. Add a syringe filter and put the liquid in the weighed vial.

5.) Weight the vial with the saturated solution. This is mass 2.

6.) Evaporate the solvent.

7.) Weigh the vial plus the solid. This is mass 3.

8.) To calculate the solubility in weight % :

Solubility = mass solid / mass saturated solution

= (mass 3 – mass 1) / (mass 2 –mass1)

Appendix V

Epimerization Experiments

1.) Enough enantiopure naproxen methyl ester is added to a vial of MeOH and set to stir at a moderate rate to allow the system to become fully saturated.

2.) After the system has equilibrated, a known amount of sodium methoxide is added and epimerization begins.

3.) The solution is sampled and analyzed via HPLC-MS using the column condition Appendix I.

Appendix VI

PRELIMINARY REPORT FOR HEIN07

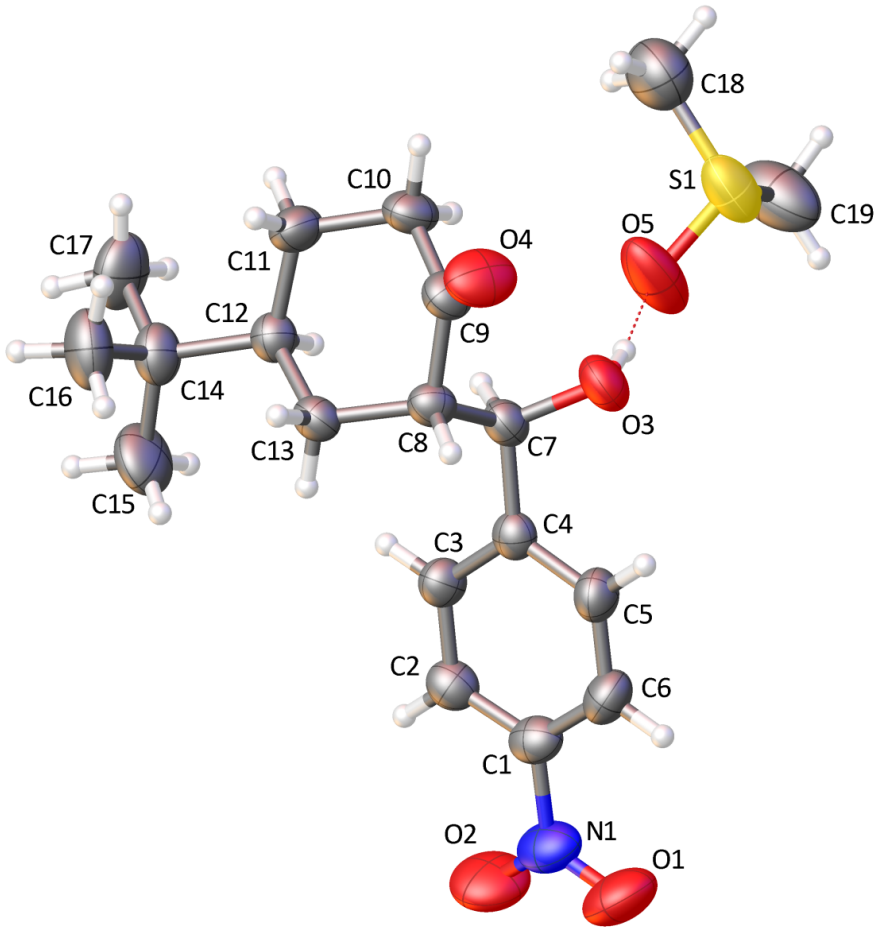

Figure 1. Preliminary structure solution of ikp-1-074 (Hein07) with ellipsoids drawn at the 50% probability level and atom labeling scheme. Note that the only one enantiomer is depicted but the sample is racemic (as noted by symmetry of space group), the other enantiomer is identical in all other aspects and thus was not depicted.

Table 1. Crystal data and structure refinement for Hein07.

Identification code	Hein07
Empirical formula	C16 H13 N5

Formula weight	275.31	
Temperature	100.0 K	
Wavelength	1.54178 Å	
Crystal system	Orthorhombic	
Space group	P b c n	
Unit cell dimensions	a = 12.6931(8) Å	α= 90°.
	b = 10.9284(6) Å	β= 90°.
	c = 18.8915(12) Å	γ = 90°.
Volume	2620.5(3) $Å^3$	
Z	8	
Density (calculated)	1.396 Mg/m^3	
Absorption coefficient	0.706 mm^{-1}	
F(000)	1152	
Crystal size	? x ? x ? mm^3	
Theta range for data collection	4.681 to 68.235°.	
Index ranges	-15<=h<=10, -11<=k<=13, -22<=l<=15	
Reflections collected	13662	
Independent reflections	2357 [R(int) = 0.0480]	
Completeness to theta = 68.000°	98.3 %	
Absorption correction	None	
Max. and min. transmission	0.7530 and 0.6314	
Refinement method	Full-matrix least-squares on F^2	
Data / restraints / parameters	2357 / 0 / 194	
Goodness-of-fit on F^2	1.059	
Final R indices [I>2sigma(I)]	R1 = 0.0349, wR2 = 0.0884	
R indices (all data)	R1 = 0.0411, wR2 = 0.0928	
Extinction coefficient	n/a	
Largest diff. peak and hole	0.134 and -0.234 $e.Å^{-3}$	

Table 2. Atomic coordinates (x 10^4) and equivalent isotropic displacement parameters ($Å^2$x 10^3) for Hein07. U(eq) is defined as one third of the trace of the orthogonalized U^{ij} tensor.

	x	y	z	U(eq)
N(1)	4779(1)	8767(1)	10576(1)	18(1)
N(2)	4732(1)	7789(1)	11031(1)	20(1)
N(3)	3948(1)	7076(1)	10886(1)	21(1)
N(4)	3460(1)	7585(1)	10315(1)	18(1)
N(5)	3668(1)	9295(1)	9576(1)	17(1)
C(1)	3978(1)	8605(1)	10134(1)	16(1)
C(2)	2464(1)	7162(1)	10005(1)	18(1)
C(3)	2368(1)	7792(1)	9300(1)	19(1)
C(4)	2904(1)	8802(1)	9117(1)	17(1)
C(5)	1561(1)	7422(1)	10516(1)	19(1)
C(6)	1373(1)	6611(1)	11067(1)	22(1)
C(7)	584(1)	6848(1)	11557(1)	26(1)
C(8)	-32(1)	7889(1)	11495(1)	26(1)
C(9)	154(1)	8703(1)	10946(1)	26(1)
C(10)	951(1)	8474(1)	10459(1)	22(1)
C(11)	2737(1)	9461(1)	8440(1)	18(1)
C(12)	1808(1)	9281(1)	8052(1)	23(1)
C(13)	1644(1)	9887(1)	7419(1)	27(1)
C(14)	2389(1)	10708(1)	7164(1)	26(1)
C(15)	3310(1)	10897(1)	7540(1)	24(1)
C(16)	3484(1)	10274(1)	8171(1)	21(1)

Table 3. Bond lengths [Å] and angles [°] for Hein07.

N(1)-N(2)	1.3731(15)	N(4)-C(2)-C(5)	109.66(10)
N(1)-C(1)	1.3274(16)	C(3)-C(2)-H(2)	108.8
N(2)-N(3)	1.2936(16)	C(3)-C(2)-C(5)	114.50(11)
N(3)-N(4)	1.3627(15)	C(5)-C(2)-H(2)	108.8
N(4)-C(1)	1.3381(16)	C(2)-C(3)-H(3)	117.8
N(4)-C(2)	1.4680(16)	C(4)-C(3)-C(2)	124.36(12)
N(5)-H(5)	0.937(18)	C(4)-C(3)-H(3)	117.8
N(5)-C(1)	1.3541(16)	N(5)-C(4)-C(11)	116.35(11)
N(5)-C(4)	1.4094(16)	C(3)-C(4)-N(5)	120.28(11)
C(2)-H(2)	1.0000	C(3)-C(4)-C(11)	123.37(12)
C(2)-C(3)	1.5035(18)	C(6)-C(5)-C(2)	119.02(12)
C(2)-C(5)	1.5250(18)	C(6)-C(5)-C(10)	119.41(12)
C(3)-H(3)	0.9500	C(10)-C(5)-C(2)	121.52(12)
C(3)-C(4)	1.3421(18)	C(5)-C(6)-H(6)	119.8
C(4)-C(11)	1.4829(17)	C(5)-C(6)-C(7)	120.30(13)
C(5)-C(6)	1.3878(19)	C(7)-C(6)-H(6)	119.8
C(5)-C(10)	1.3905(19)	C(6)-C(7)-H(7)	119.8
C(6)-H(6)	0.9500	C(8)-C(7)-C(6)	120.32(13)
C(6)-C(7)	1.3879(19)	C(8)-C(7)-H(7)	119.8
C(7)-H(7)	0.9500	C(7)-C(8)-H(8)	120.2
C(7)-C(8)	1.386(2)	C(7)-C(8)-C(9)	119.51(13)
C(8)-H(8)	0.9500	C(9)-C(8)-H(8)	120.2
C(8)-C(9)	1.387(2)	C(8)-C(9)-H(9)	119.8
C(9)-H(9)	0.9500	C(8)-C(9)-C(10)	120.31(13)
C(9)-C(10)	1.3899(19)	C(10)-C(9)-H(9)	119.8
C(10)-H(10)	0.9500	C(5)-C(10)-H(10)	119.9
C(11)-C(12)	1.4018(18)	C(9)-C(10)-C(5)	120.14(13)
C(11)-C(16)	1.3955(18)	C(9)-C(10)-H(10)	119.9
C(12)-H(12)	0.9500	C(12)-C(11)-C(4)	120.16(12)
C(12)-C(13)	1.3831(19)	C(16)-C(11)-C(4)	121.75(12)
C(13)-H(13)	0.9500	C(16)-C(11)-C(12)	118.09(12)
C(13)-C(14)	1.390(2)	C(11)-C(12)-H(12)	119.6
C(14)-H(14)	0.9500	C(13)-C(12)-C(11)	120.73(13)
C(14)-C(15)	1.3832(19)	C(13)-C(12)-H(12)	119.6
C(15)-H(15)	0.9500	C(12)-C(13)-H(13)	119.8
C(15)-C(16)	1.3896(19)	C(12)-C(13)-C(14)	120.45(13)
C(16)-H(16)	0.9500	C(14)-C(13)-H(13)	119.8
		C(13)-C(14)-H(14)	120.2
C(1)-N(1)-N(2)	104.90(10)	C(15)-C(14)-C(13)	119.53(12)
N(3)-N(2)-N(1)	111.65(10)	C(15)-C(14)-H(14)	120.2
N(2)-N(3)-N(4)	105.77(10)	C(14)-C(15)-H(15)	119.9
N(3)-N(4)-C(2)	125.35(10)	C(14)-C(15)-C(16)	120.14(13)
C(1)-N(4)-N(3)	108.60(10)	C(16)-C(15)-H(15)	119.9
C(1)-N(4)-C(2)	125.69(11)	C(11)-C(16)-H(16)	119.5
C(1)-N(5)-H(5)	115.6(10)	C(15)-C(16)-C(11)	121.04(12)
C(1)-N(5)-C(4)	117.77(10)	C(15)-C(16)-H(16)	119.5
C(4)-N(5)-H(5)	123.3(10)		
N(1)-C(1)-N(4)	109.07(11)		
N(1)-C(1)-N(5)	129.58(11)		
N(4)-C(1)-N(5)	121.35(11)		
N(4)-C(2)-H(2)	108.8		
N(4)-C(2)-C(3)	106.17(10)		

Table 4. Anisotropic displacement parameters ($Å^2 x\ 10^3$) for Hein07. The anisotropic displacement factor exponent takes the form: $-2\pi^2[\ h^2\ a^{*2}U^{11} + ...\ + 2\ h\ k\ a^*\ b^*\ U^{12}\ ]$

	U^{11}	U^{22}	U^{33}	U^{23}	U^{13}	U^{12}
N(1)	18(1)	20(1)	16(1)	2(1)	-1(1)	0(1)
N(2)	18(1)	21(1)	20(1)	4(1)	-1(1)	0(1)
N(3)	18(1)	23(1)	20(1)	4(1)	-2(1)	0(1)
N(4)	17(1)	18(1)	17(1)	2(1)	-2(1)	-1(1)
N(5)	19(1)	18(1)	16(1)	1(1)	-3(1)	-2(1)
C(1)	16(1)	16(1)	16(1)	-1(1)	1(1)	1(1)
C(2)	18(1)	18(1)	19(1)	-2(1)	-2(1)	-4(1)
C(3)	17(1)	22(1)	18(1)	-2(1)	-2(1)	-2(1)
C(4)	15(1)	21(1)	15(1)	-4(1)	0(1)	2(1)
C(5)	18(1)	21(1)	17(1)	-2(1)	-3(1)	-6(1)
C(6)	23(1)	22(1)	21(1)	0(1)	-1(1)	-5(1)
C(7)	29(1)	30(1)	20(1)	0(1)	1(1)	-11(1)
C(8)	20(1)	37(1)	22(1)	-8(1)	2(1)	-6(1)
C(9)	22(1)	31(1)	24(1)	-5(1)	-4(1)	2(1)
C(10)	21(1)	25(1)	20(1)	1(1)	-3(1)	-1(1)
C(11)	19(1)	19(1)	16(1)	-3(1)	0(1)	4(1)
C(12)	20(1)	25(1)	23(1)	0(1)	-1(1)	1(1)
C(13)	24(1)	33(1)	23(1)	-1(1)	-6(1)	5(1)
C(14)	32(1)	27(1)	18(1)	2(1)	-2(1)	8(1)
C(15)	29(1)	23(1)	20(1)	1(1)	1(1)	1(1)
C(16)	22(1)	21(1)	19(1)	-2(1)	-2(1)	0(1)

Table 5. Hydrogen coordinates (x 10^4) and isotropic displacement parameters ($Å^2$x 10^3) for Hein07.

	x	y	z	U(eq)
H(5)	4132(13)	9922(16)	9444(8)	35(4)
H(2)	2508	6259	9925	22
H(3)	1897	7452	8963	23
H(6)	1786	5889	11109	27
H(7)	466	6294	11936	32
H(8)	-579	8045	11827	32
H(9)	-264	9419	10903	31
H(10)	1079	9037	10086	26
H(12)	1285	8737	8227	27
H(13)	1018	9741	7157	32
H(14)	2267	11137	6734	31
H(15)	3823	11454	7367	29
H(16)	4123	10403	8422	25

Table 6. Hydrogen bonds for Hein07 [Å and °].

D-H...A	d(D-H)	d(H...A)	d(D...A)	<(DHA)
N(5)-H(5)...N(1)#1	0.937(18)	1.991(18)	2.9075(15)	165.3(14)

Symmetry transformations used to generate equivalent atoms:
#1 -x+1,-y+2,-z+2

Hein11 XRD Report
Sample: JEG-1-174-freebase
Analysis and Report by: Christopher J. A. Daley

University of California, San Diego
Department of Chemistry and Biochemistry
Small Molecule X-ray Crystallography Facility
5128 Urey Hall MC 0358
La Jolla CA, 92093-0358

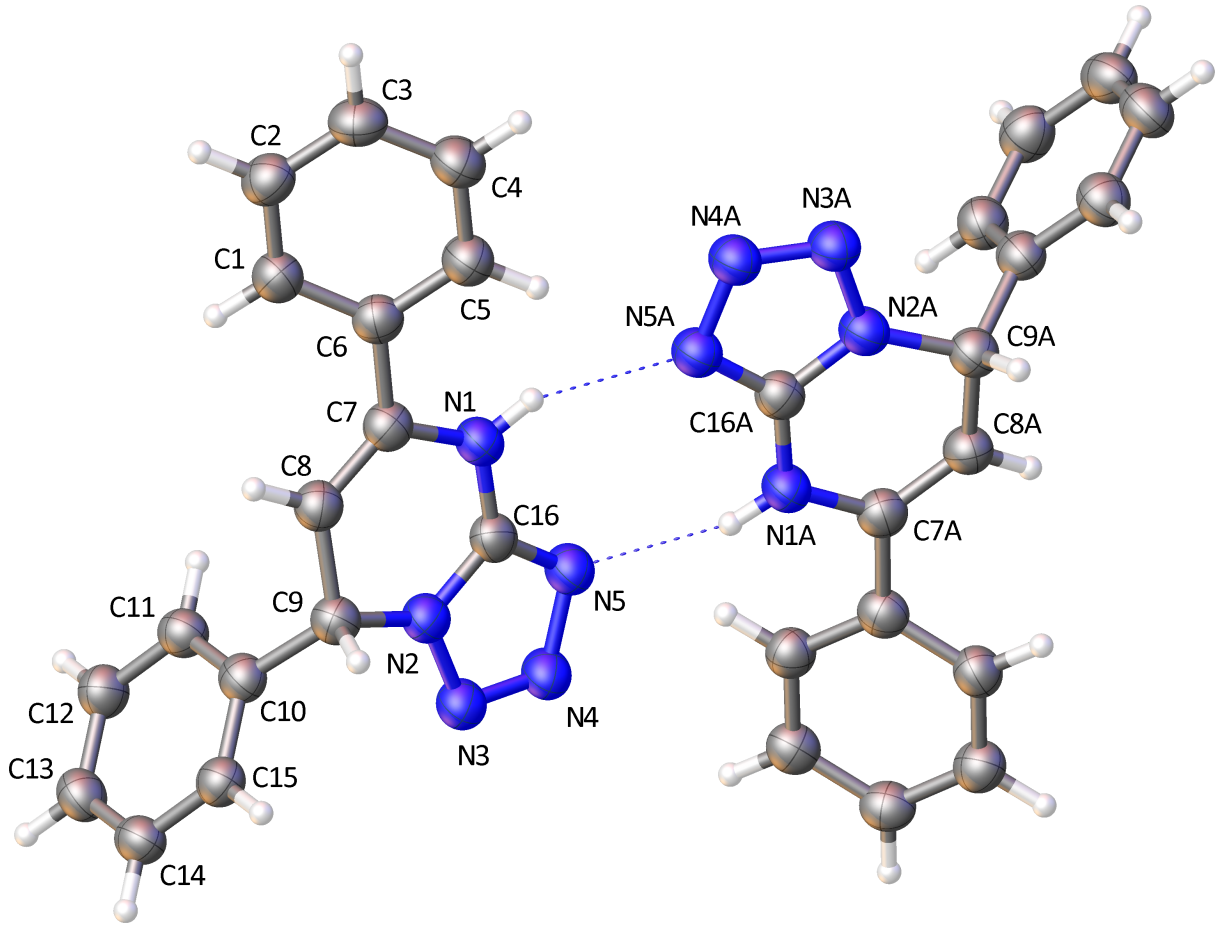

Figure 1. Ortep diagram of JEH-1-174-freebase (Hein11) showing ellipsoids at 50% probability and atom labeling scheme.

Experimental Summary

The single crystal X-ray diffraction studies were carried out on a Bruker APEX CCD diffractometer equipped with Cu K_a radiation (l = 1. 54178). A 0.351 x 0.202 x 0.140 mm clear colorless block was mounted on a Cryoloop with Paratone oil. Data were collected in a nitrogen gas stream at 100(2) K using f and w scans. Crystal-to-detector distance was 40 mm using 1-3 s exposure times with a scan width of 1.0°. Data collection was 100.0% complete to 68.000° in *q*. A total of 21873 reflections were collected covering the indices, -10<=h<=10, -10<=k<=10, -21<=l<=21. 4926 reflections were found to be symmetry independent, with a R_{int} of 0.0345. Indexing and unit cell refinement indicated a primitive, monoclinic lattice. The space group was found to be $P2_1$. The data were integrated using the Bruker SAINT software program and scaled using the SADABS software program. Solution by direct methods (SHELXT) produced a complete phasing model consistent with the proposed structure.

All nonhydrogen atoms were refined anisotropically by full-matrix least-squares (SHELXL). The amine hydrogen atom was found via the difference map and the bond distance was restrained relative to the parent oxygen atom using the appropriate DFIX command in SHELXL. All remaining hydrogen atoms were placed using a riding model. Their positions were constrained relative to their parent atom using the appropriate HFIX command in SHELXL. Crystallographic data are summarized in Table 1.

Table 1. Crystal data and structure refinement for Hein11.

Identification code	JEH-1-174-freebase
Empirical formula	C16 H13 N5
Molecular formula	C16 H13 N5
Formula weight	275.31
Temperature	100.0 K
Wavelength	1.54178 Å

Crystal system	Monoclinic	
Space group	P 1 21 1	
Unit cell dimensions	a = 8.7736(2) Å	α= 90°.
	b = 8.8396(2) Å	β= 98.8220(9)°.
	c = 17.6810(4) Å	γ = 90°.
Volume	1355.03(5) $Å^3$	
Z	4	
Density (calculated)	1.350 Mg/m^3	
Absorption coefficient	0.682 mm^{-1}	
F(000)	576	
Crystal size	0.351 x 0.202 x 0.14 mm^3	
Crystal color, habit	Clear colorless Block	
Theta range for data collection	2.529 to 68.238°.	
Index ranges	-10<=h<=10, -10<=k<=10, -21<=l<=21	
Reflections collected	21873	
Independent reflections	4926 [R(int) = 0.0345]	
Completeness to theta = 68.000°	100.0 %	
Absorption correction	Semi-empirical from equivalents	
Max. and min. transmission	0.0818 and 0.0108	
Refinement method	Full-matrix least-squares on F^2	
Data / restraints / parameters	4926 / 1 / 387	
Goodness-of-fit on F^2	1.077	
Final R indices [I>2sigma(I)]	R1 = 0.0542, wR2 = 0.1194	
R indices (all data)	R1 = 0.0548, wR2 = 0.1206	
Absolute structure parameter	0.04(13)	
Extinction coefficient	n/a	
Largest diff. peak and hole	0.369 and -0.162 e.$Å^{-3}$	

Table 2. Atomic coordinates (x 10^4) and equivalent isotropic displacement parameters ($Å^2$x 10^3) for Hein11. U(eq) is defined as one third of the trace of the orthogonalized U^{ij} tensor.

	x	y	z	U(eq)
N(1)	1241(2)	7357(3)	2082(1)	44(1)
N(2)	1544(2)	7090(2)	794(1)	43(1)
N(3)	2314(2)	6164(3)	370(1)	47(1)
N(4)	3068(3)	5225(3)	842(1)	48(1)
N(5)	2824(2)	5492(3)	1578(1)	46(1)
C(1)	-730(3)	10885(3)	2498(2)	47(1)
C(2)	-1410(3)	11537(3)	3074(2)	50(1)
C(3)	-1741(3)	10677(4)	3681(2)	51(1)
C(4)	-1382(3)	9151(4)	3714(2)	53(1)
C(5)	-705(3)	8486(3)	3134(2)	49(1)
C(6)	-369(3)	9346(3)	2518(1)	43(1)
C(7)	289(3)	8631(3)	1880(1)	42(1)
C(8)	-12(3)	9102(3)	1151(1)	43(1)
C(9)	427(3)	8252(3)	472(1)	42(1)
C(10)	1090(3)	9162(3)	-127(1)	42(1)
C(11)	2279(3)	10198(3)	67(1)	44(1)
C(12)	2929(3)	10926(3)	-501(2)	47(1)
C(13)	2374(3)	10641(3)	-1267(2)	48(1)
C(14)	1189(3)	9613(3)	-1464(1)	46(1)
C(15)	552(3)	8874(3)	-896(1)	44(1)
C(16)	1852(3)	6651(3)	1524(1)	42(1)
N(1A)	2796(3)	3097(3)	2706(1)	46(1)
N(2A)	1962(2)	2931(3)	3903(1)	44(1)
N(3A)	1134(3)	3784(3)	4332(1)	48(1)
N(4A)	776(3)	5003(3)	3950(1)	48(1)
N(5A)	1334(2)	4997(3)	3269(1)	45(1)
C(1A)	4542(3)	-403(3)	2123(2)	45(1)
C(2A)	5287(3)	-939(3)	1546(2)	48(1)
C(3A)	5921(3)	54(3)	1067(1)	46(1)
C(4A)	5795(3)	1605(3)	1179(1)	46(1)
C(5A)	5040(3)	2156(3)	1756(1)	44(1)
C(6A)	4401(3)	1156(3)	2237(1)	44(1)
C(7A)	3557(3)	1710(3)	2846(1)	43(1)
C(8A)	3471(3)	932(3)	3492(1)	45(1)
C(9A)	2507(3)	1381(3)	4093(1)	44(1)
C(10A)	3383(3)	1305(3)	4906(1)	45(1)
C(11A)	4812(3)	1996(3)	5090(2)	49(1)
C(12A)	5608(3)	1912(3)	5835(2)	54(1)
C(13A)	4957(3)	1140(4)	6393(2)	56(1)
C(14A)	3542(3)	456(4)	6209(2)	56(1)
C(15A)	2745(3)	526(3)	5464(2)	50(1)
C(16A)	2063(3)	3686(3)	3257(1)	42(1)

Table 3. Bond lengths [Å] and angles [°] for Hein11.

N(1)-H(1)	0.84(4)	C(4A)-C(5A)	1.387(4)
N(1)-C(7)	1.414(3)	C(5A)-H(5A)	0.9500
N(1)-C(16)	1.346(3)	C(5A)-C(6A)	1.401(3)
N(2)-N(3)	1.357(3)	C(6A)-C(7A)	1.480(3)
N(2)-C(9)	1.473(3)	C(7A)-C(8A)	1.345(4)
N(2)-C(16)	1.336(3)	C(8A)-H(8A)	0.9500
N(3)-N(4)	1.287(3)	C(8A)-C(9A)	1.510(3)
N(4)-N(5)	1.371(3)	C(9A)-H(9A)	1.0000
N(5)-C(16)	1.326(3)	C(9A)-C(10A)	1.524(3)
C(1)-H(1A)	0.9500	C(10A)-C(11A)	1.388(4)
C(1)-C(2)	1.382(4)	C(10A)-C(15A)	1.390(3)
C(1)-C(6)	1.396(4)	C(11A)-H(11A)	0.9500
C(2)-H(2)	0.9500	C(11A)-C(12A)	1.396(4)
C(2)-C(3)	1.382(4)	C(12A)-H(12A)	0.9500
C(3)-H(3)	0.9500	C(12A)-C(13A)	1.392(4)
C(3)-C(4)	1.385(4)	C(13A)-H(13A)	0.9500
C(4)-H(4)	0.9500	C(13A)-C(14A)	1.374(5)
C(4)-C(5)	1.392(4)	C(14A)-H(14A)	0.9500
C(5)-H(5)	0.9500	C(14A)-C(15A)	1.394(4)
C(5)-C(6)	1.396(4)	C(15A)-H(15A)	0.9500
C(6)-C(7)	1.485(3)		
C(7)-C(8)	1.341(4)	C(7)-N(1)-H(1)	123(2)
C(8)-H(8)	0.9500	C(16)-N(1)-H(1)	117(3)
C(8)-C(9)	1.516(3)	C(16)-N(1)-C(7)	118.1(2)
C(9)-H(9)	1.0000	N(3)-N(2)-C(9)	124.36(19)
C(9)-C(10)	1.515(3)	C(16)-N(2)-N(3)	108.4(2)
C(10)-C(11)	1.391(4)	C(16)-N(2)-C(9)	126.9(2)
C(10)-C(15)	1.392(3)	N(4)-N(3)-N(2)	106.25(19)
C(11)-H(11)	0.9500	N(3)-N(4)-N(5)	111.4(2)
C(11)-C(12)	1.387(3)	C(16)-N(5)-N(4)	104.9(2)
C(12)-H(12)	0.9500	C(2)-C(1)-H(1A)	119.7
C(12)-C(13)	1.391(4)	C(2)-C(1)-C(6)	120.7(2)
C(13)-H(13)	0.9500	C(6)-C(1)-H(1A)	119.7
C(13)-C(14)	1.384(4)	C(1)-C(2)-H(2)	119.7
C(14)-H(14)	0.9500	C(3)-C(2)-C(1)	120.6(2)
C(14)-C(15)	1.386(4)	C(3)-C(2)-H(2)	119.7
C(15)-H(15)	0.9500	C(2)-C(3)-H(3)	120.2
N(1A)-H(1AA)	0.84(4)	C(2)-C(3)-C(4)	119.7(2)
N(1A)-C(7A)	1.399(4)	C(4)-C(3)-H(3)	120.2
N(1A)-C(16A)	1.351(3)	C(3)-C(4)-H(4)	120.0
N(2A)-N(3A)	1.356(3)	C(3)-C(4)-C(5)	120.0(3)
N(2A)-C(9A)	1.473(3)	C(5)-C(4)-H(4)	120.0
N(2A)-C(16A)	1.338(3)	C(4)-C(5)-H(5)	119.7
N(3A)-N(4A)	1.285(3)	C(4)-C(5)-C(6)	120.7(3)
N(4A)-N(5A)	1.367(3)	C(6)-C(5)-H(5)	119.7
N(5A)-C(16A)	1.326(4)	C(1)-C(6)-C(5)	118.4(2)
C(1A)-H(1AB)	0.9500	C(1)-C(6)-C(7)	120.6(2)
C(1A)-C(2A)	1.377(4)	C(5)-C(6)-C(7)	120.9(2)
C(1A)-C(6A)	1.401(4)	N(1)-C(7)-C(6)	115.5(2)
C(2A)-H(2A)	0.9500	C(8)-C(7)-N(1)	120.8(2)
C(2A)-C(3A)	1.394(4)	C(8)-C(7)-C(6)	123.7(2)
C(3A)-H(3A)	0.9500	C(7)-C(8)-H(8)	117.6
C(3A)-C(4A)	1.392(4)	C(7)-C(8)-C(9)	124.8(2)
C(4A)-H(4A)	0.9500	C(9)-C(8)-H(8)	117.6

N(2)-C(9)-C(8)	105.94(18)
N(2)-C(9)-H(9)	107.8
N(2)-C(9)-C(10)	109.68(18)
C(8)-C(9)-H(9)	107.8
C(10)-C(9)-C(8)	117.5(2)
C(10)-C(9)-H(9)	107.8
C(11)-C(10)-C(9)	122.1(2)
C(11)-C(10)-C(15)	119.4(2)
C(15)-C(10)-C(9)	118.4(2)
C(10)-C(11)-H(11)	119.9
C(12)-C(11)-C(10)	120.2(2)
C(12)-C(11)-H(11)	119.9
C(11)-C(12)-H(12)	120.0
C(11)-C(12)-C(13)	120.0(2)
C(13)-C(12)-H(12)	120.0
C(12)-C(13)-H(13)	120.0
C(14)-C(13)-C(12)	120.1(2)
C(14)-C(13)-H(13)	120.0
C(13)-C(14)-H(14)	120.1
C(13)-C(14)-C(15)	119.9(2)
C(15)-C(14)-H(14)	120.1
C(10)-C(15)-H(15)	119.8
C(14)-C(15)-C(10)	120.5(2)
C(14)-C(15)-H(15)	119.8
N(2)-C(16)-N(1)	121.9(2)
N(5)-C(16)-N(1)	129.1(2)
N(5)-C(16)-N(2)	109.0(2)
C(7A)-N(1A)-H(1AA)	123(3)
C(16A)-N(1A)-H(1AA)	118(3)
C(16A)-N(1A)-C(7A)	118.5(2)
N(3A)-N(2A)-C(9A)	124.9(2)
C(16A)-N(2A)-N(3A)	108.1(2)
C(16A)-N(2A)-C(9A)	126.6(2)
N(4A)-N(3A)-N(2A)	106.32(19)
N(3A)-N(4A)-N(5A)	111.6(2)
C(16A)-N(5A)-N(4A)	104.9(2)
C(2A)-C(1A)-H(1AB)	119.7
C(2A)-C(1A)-C(6A)	120.5(2)
C(6A)-C(1A)-H(1AB)	119.7
C(1A)-C(2A)-H(2A)	119.6
C(1A)-C(2A)-C(3A)	120.8(2)
C(3A)-C(2A)-H(2A)	119.6
C(2A)-C(3A)-H(3A)	120.5
C(4A)-C(3A)-C(2A)	119.0(2)
C(4A)-C(3A)-H(3A)	120.5
C(3A)-C(4A)-H(4A)	119.7
C(5A)-C(4A)-C(3A)	120.6(2)
C(5A)-C(4A)-H(4A)	119.7
C(4A)-C(5A)-H(5A)	119.8
C(4A)-C(5A)-C(6A)	120.3(2)
C(6A)-C(5A)-H(5A)	119.8
C(1A)-C(6A)-C(5A)	118.8(2)
C(1A)-C(6A)-C(7A)	119.7(2)
C(5A)-C(6A)-C(7A)	121.5(2)
N(1A)-C(7A)-C(6A)	116.1(2)
C(8A)-C(7A)-N(1A)	120.7(2)
C(8A)-C(7A)-C(6A)	123.2(2)
C(7A)-C(8A)-H(8A)	117.5
C(7A)-C(8A)-C(9A)	125.0(2)
C(9A)-C(8A)-H(8A)	117.5
N(2A)-C(9A)-C(8A)	106.3(2)
N(2A)-C(9A)-H(9A)	108.7
N(2A)-C(9A)-C(10A)	110.8(2)
C(8A)-C(9A)-H(9A)	108.7
C(8A)-C(9A)-C(10A)	113.40(19)
C(10A)-C(9A)-H(9A)	108.7
C(11A)-C(10A)-C(9A)	120.5(2)
C(11A)-C(10A)-C(15A)	120.0(2)
C(15A)-C(10A)-C(9A)	119.5(2)
C(10A)-C(11A)-H(11A)	120.0
C(10A)-C(11A)-C(12A)	120.1(2)
C(12A)-C(11A)-H(11A)	120.0
C(11A)-C(12A)-H(12A)	120.2
C(13A)-C(12A)-C(11A)	119.7(3)
C(13A)-C(12A)-H(12A)	120.2
C(12A)-C(13A)-H(13A)	120.0
C(14A)-C(13A)-C(12A)	120.1(2)
C(14A)-C(13A)-H(13A)	120.0
C(13A)-C(14A)-H(14A)	119.7
C(13A)-C(14A)-C(15A)	120.6(3)
C(15A)-C(14A)-H(14A)	119.7
C(10A)-C(15A)-C(14A)	119.6(2)
C(10A)-C(15A)-H(15A)	120.2
C(14A)-C(15A)-H(15A)	120.2
N(2A)-C(16A)-N(1A)	121.6(2)
N(5A)-C(16A)-N(1A)	129.3(2)
N(5A)-C(16A)-N(2A)	109.1(2)

Table 4. Anisotropic displacement parameters ($Å^2 x\ 10^3$) for Hein11. The anisotropic displacement factor exponent takes the form: $-2\pi^2[\ h^2\ a^{*2}U^{11} + ...\ + 2\ h\ k\ a^*\ b^*\ U^{12}\ ]$

	U^{11}	U^{22}	U^{33}	U^{23}	U^{13}	U^{12}
N(1)	49(1)	44(1)	39(1)	3(1)	9(1)	2(1)
N(2)	47(1)	42(1)	42(1)	2(1)	11(1)	1(1)
N(3)	52(1)	45(1)	45(1)	2(1)	14(1)	2(1)
N(4)	54(1)	45(1)	46(1)	4(1)	17(1)	5(1)
N(5)	49(1)	45(1)	44(1)	4(1)	12(1)	5(1)
C(1)	50(1)	46(1)	44(1)	1(1)	6(1)	1(1)
C(2)	52(1)	47(1)	51(1)	-3(1)	6(1)	6(1)
C(3)	51(1)	58(2)	46(1)	-7(1)	12(1)	4(1)
C(4)	60(1)	56(2)	45(1)	3(1)	15(1)	1(1)
C(5)	54(1)	47(1)	46(1)	1(1)	10(1)	3(1)
C(6)	42(1)	45(1)	42(1)	-2(1)	5(1)	-1(1)
C(7)	41(1)	42(1)	45(1)	0(1)	8(1)	-1(1)
C(8)	43(1)	42(1)	45(1)	1(1)	9(1)	1(1)
C(9)	42(1)	44(1)	41(1)	0(1)	6(1)	0(1)
C(10)	42(1)	41(1)	42(1)	2(1)	8(1)	4(1)
C(11)	45(1)	45(1)	41(1)	0(1)	5(1)	3(1)
C(12)	46(1)	46(1)	50(1)	2(1)	9(1)	-2(1)
C(13)	50(1)	49(1)	45(1)	7(1)	13(1)	2(1)
C(14)	52(1)	48(1)	39(1)	1(1)	6(1)	5(1)
C(15)	46(1)	41(1)	44(1)	-1(1)	7(1)	2(1)
C(16)	44(1)	40(1)	42(1)	2(1)	8(1)	-3(1)
N(1A)	53(1)	45(1)	41(1)	3(1)	13(1)	4(1)
N(2A)	45(1)	47(1)	41(1)	1(1)	8(1)	3(1)
N(3A)	52(1)	50(1)	44(1)	0(1)	11(1)	5(1)
N(4A)	51(1)	50(1)	43(1)	2(1)	10(1)	6(1)
N(5A)	47(1)	46(1)	41(1)	2(1)	9(1)	3(1)
C(1A)	48(1)	45(1)	44(1)	4(1)	9(1)	0(1)
C(2A)	48(1)	46(1)	49(1)	0(1)	7(1)	6(1)
C(3A)	41(1)	54(1)	45(1)	-2(1)	9(1)	4(1)
C(4A)	42(1)	52(1)	45(1)	1(1)	7(1)	-2(1)
C(5A)	44(1)	43(1)	45(1)	0(1)	6(1)	-1(1)
C(6A)	42(1)	48(1)	41(1)	1(1)	4(1)	1(1)
C(7A)	44(1)	43(1)	43(1)	-2(1)	6(1)	-1(1)
C(8A)	49(1)	44(1)	42(1)	0(1)	9(1)	3(1)
C(9A)	47(1)	44(1)	43(1)	1(1)	9(1)	1(1)
C(10A)	49(1)	43(1)	43(1)	1(1)	10(1)	6(1)
C(11A)	54(1)	47(1)	48(1)	3(1)	11(1)	1(1)
C(12A)	53(1)	50(1)	58(1)	-2(1)	2(1)	1(1)
C(13A)	66(2)	56(2)	43(1)	0(1)	3(1)	14(1)
C(14A)	65(2)	59(2)	44(1)	9(1)	13(1)	7(1)
C(15A)	51(1)	53(1)	48(1)	3(1)	11(1)	2(1)
C(16A)	42(1)	44(1)	41(1)	0(1)	6(1)	-1(1)

Table 5. Hydrogen coordinates (x 10^4) and isotropic displacement parameters ($Å^2$x 10^{3}) for Hein11.

	x	y	z	U(eq)
H(1)	1280(40)	6900(40)	2500(20)	54(9)
H(1A)	-506	11491	2085	56
H(2)	-1652	12585	3052	60
H(3)	-2212	11131	4074	61
H(4)	-1598	8557	4133	64
H(5)	-469	7436	3157	59
H(8)	-540	10037	1054	52
H(9)	-515	7721	211	51
H(11)	2646	10408	590	53
H(12)	3754	11619	-367	57
H(13)	2808	11151	-1656	57
H(14)	813	9415	-1988	56
H(15)	-258	8165	-1032	52
H(1AA)	2870(40)	3640(50)	2320(20)	54(9)
H(1AB)	4120	-1095	2446	55
H(2A)	5370	-1999	1474	58
H(3A)	6431	-322	669	56
H(4A)	6229	2292	858	56
H(5A)	4956	3217	1826	53
H(8A)	4061	30	3576	54
H(9A)	1593	693	4054	53
H(11A)	5249	2526	4708	59
H(12A)	6589	2379	5961	65
H(13A)	5492	1086	6902	67
H(14A)	3104	-69	6592	67
H(15A)	1771	44	5340	61

Table 6. Hydrogen bonds for Hein11 [Å and °].

D-H...A	d(D-H)	d(H...A)	d(D...A)	<(DHA)
N(1)-H(1)...N(5A)	0.84(4)	2.16(4)	2.952(3)	157(3)
N(1A)-H(1AA)...N(5)	0.84(4)	2.10(4)	2.912(3)	163(4)

.